

HELIUM RESOURCES OF MARE TRANQUILLITATIS

WCSAR-TR-AR3-9207-1

Technical Report



**Wisconsin Center for
Space Automation and Robotics**



**A NASA supported Center for
the Commercial Development of Space**

Helium Resources of Mare Tranquillitatis

Eugene N. Cameron

Wisconsin Center for Space Automation and Robotics
University of Wisconsin-Madison
1357 Johnson Drive
Madison, WI 53706

July 1992

TABLE OF CONTENTS

| | Page |
|---|------|
| INTRODUCTION | 1 |
| SOURCES OF INFORMATION | 1 |
| MARE TRANQUILLITATIS | 2 |
| General Description | 2 |
| Pre-mare Features | 5 |
| Mare Features | 10 |
| General Statement | 10 |
| Ridges | 10 |
| Rilles | 10 |
| Domes | 10 |
| Basement Islands | 11 |
| Craters | 11 |
| Ejecta Blankets | 11 |
| Ray Materials | 14 |
| The Mare Regolith | 16 |
| General Description | 16 |
| Modal Composition | 16 |
| Grain (Particle) Size | 18 |
| Structure of the Regolith | 19 |
| Thickness of the Regolith | 19 |
| Helium Content of the Regolith | 22 |
| MINABLE AREAS IN MARE TRANQUILLITATIS | 27 |
| General Statement | 27 |
| Percentage of the Mare Occupied by High TiO ₂ Regolith | 29 |
| Percentage of the Mare Physically Amenable to Mining | 39 |
| General Remarks | 39 |
| Information from Geologic Maps | 39 |
| Minaible Areas as Determined from High-Resolution Photographs | 41 |
| Measurements | 44 |
| Other Factors Affecting Minability | 48 |
| Amount of Helium in Minaible Regolith | 56 |
| OTHER AREAS OF HIGH-TITANIUM REGOLITH | 56 |
| SUMMARY AND CONCLUSIONS | 58 |
| ACKNOWLEDGMENTS | 60 |
| REFERENCES | 61 |

INTRODUCTION

Since 1987 the writer has been engaged in a series of studies of the geology and helium resources of Mare Tranquillitatis, selected as the most promising first site for helium mining based on results of the various Apollo missions and on the results of remote sensing of the Moon. Preliminary reports (Cameron, 1987, 1988) were followed by a comprehensive report (Cameron, 1990), the bulk of which has since been published in a paper by Cameron and Kulcinski (1992). The present report is a revision of the 1990 report, incorporating the results of further study of Tranquillitatis and new information on the mare that has become available.

The study of Tranquillitatis has had a sixfold purpose: (1) to delineate areas of high-Ti regolith in the mare, (2) to evaluate information on the helium content of the regolith, (3) to estimate the average depth of regolith, (4) to examine features of the mare that will determine the ease or difficulty of mining and place constraints on mining methods and equipment, (5) to estimate the percentage of the mare that will be minable and the amount of He-3 present in it, and (6) to formulate recommendations for further work needed to verify the helium potential of the mare. The first five topics are discussed in this report. The sixth topic will be the subject of a separate report.

SOURCES OF INFORMATION

The following are the principal sources of information utilized in preparing this report:

- A. U.S. Geological Survey, Geologic Atlas of the Moon. A series of photogeologic maps.
 - 1) Carr, M.H., 1966, Mare Serenitatis quadrangle. Map I-489 (LAC-42), scale 1:1,000,000.
 - 2) Morris, E.C., and D.E. Wilhelms, 1967, Julius Caesar quadrangle. Map I-510 (LAC-60), scale 1:1,000,000.
 - 3) Wilhelms, D.E., 1972, Taruntius quadrangle. Map I-722 (LAC-61), scale 1:1,000,000.
 - 4) Scott, D.H., and H.A. Pohn, 1972, Macrobius quadrangle. Map I-789 (LAC-43), scale 1:1,000,000.

- 5) Milton, D.J., 1968, Theophilus quadrangle. Map I-546 (LAC-78), scale 1:1,000,000.
 - 6) Elston, D.P., 1972, Colombo quadrangle. Map I-714 (LAC-79), scale 1:1,000,000.
 - 7) Grolier, M.J., 1970, Sabine D region. Map I-618 [ORB II-6 (100)], scale 1:100,000.
 - 8) Grolier, M.J., 1970, Apollo Landing Site II (Apollo 11). Map I-619 [ORB II-6 (25)], scale 1:25,000.
- B. Lunar Orbiter II medium-resolution photographs 76M to 91M and 67M-74M; high-resolution photographs 76H to 91H and 67H to 74H.
 - C. Shoemaker, E.M., and others, 1969, Chap. 3 of Apollo 11 Preliminary Science Report. NASA Report SP-214, pp. 41-83.
 - D. Shoemaker, E.M., and others, 1967, Chap. 3, Surveyor V mission report. JPL, Tech. Report 32-1246.
 - E. Wilhelms, D.E., 1987, Geologic History of the Moon. U.S. Geol. Survey, Prof. Paper 1348, Washington, D.C., 302 pp.
 - F. Proceedings of the successive Lunar Science Conferences and Lunar and Planetary Science Conferences.

Specific references to these and other sources of information are given at appropriate places in the text.

MARE TRANQUILLITATIS

General Description

Mare Tranquillitatis (Fig. 1) occupies a large basin, irregular in outline, formed by a major impact during Pre-Nectarian time (Fig. 2). In Upper Imbrian time the basin was flooded by flows of basaltic lava, probably accompanied by late falls of volcanic ash. The mare is completely covered (Fig. 1) by maps 1) to 6) of the above list. Most of the mare lies in the Julius Caesar and Taruntius quadrangles. On the two quadrangle maps, three major units have been recognized in the mare, largely on the basis of albedo as observed telescopically from Earth. From oldest to youngest, these are designated on the various geologic maps as Im-1, Im-2, and Im-3, or as Ipm-1, Ipm-2, and Ipm-3. There is some confusion as to the distribution of the three units.

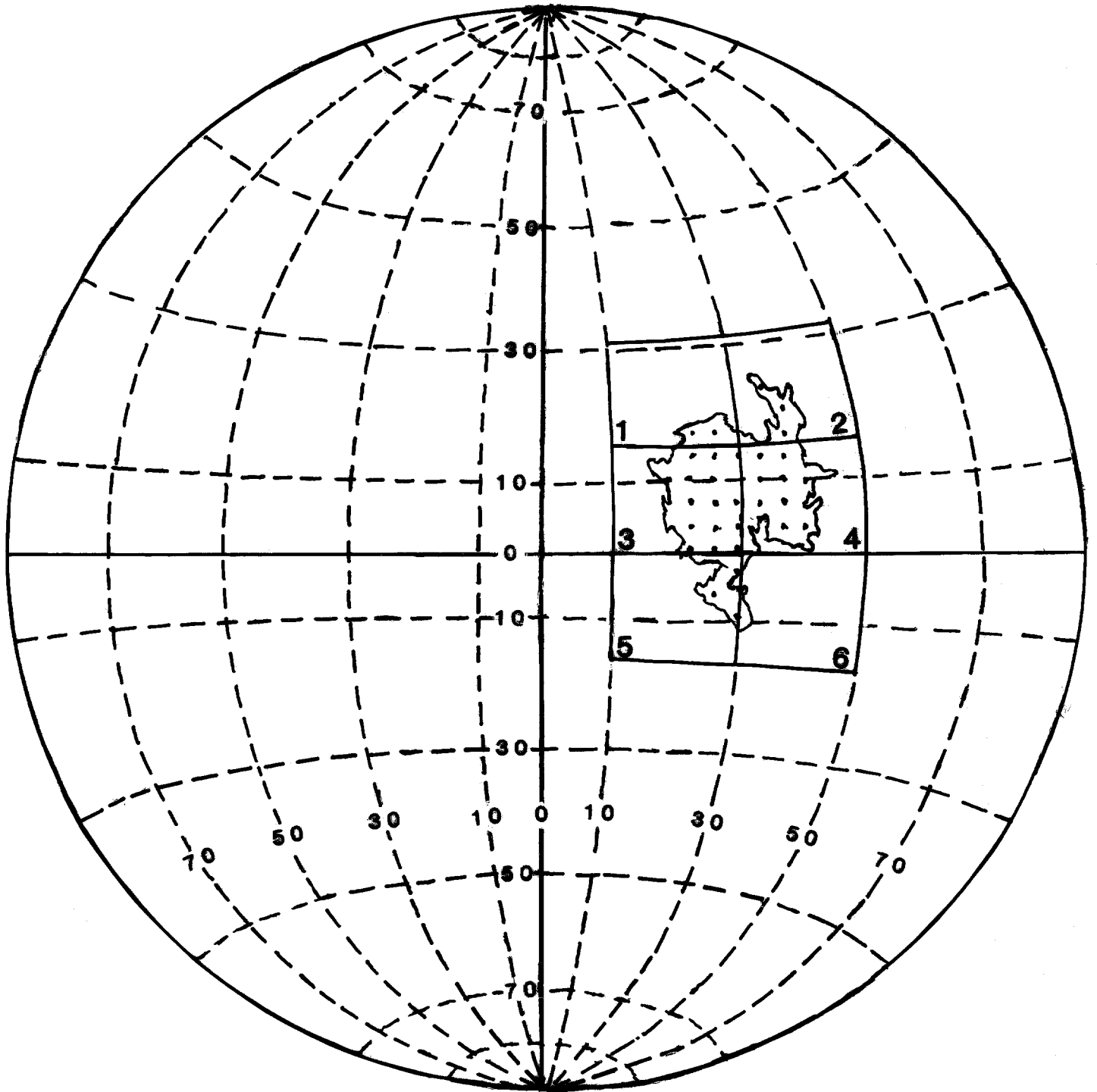


Fig. 1. Index map of the near side of the Moon, showing coverage of Mare Tranquillitatis (stippled area) by quadrangle geologic maps. 1 - Mare Serenitatis; 2 - Macrobius; 3 - Julius Caesar; 4 - Taruntius; 5 - Theophilus; 6 - Colombo.

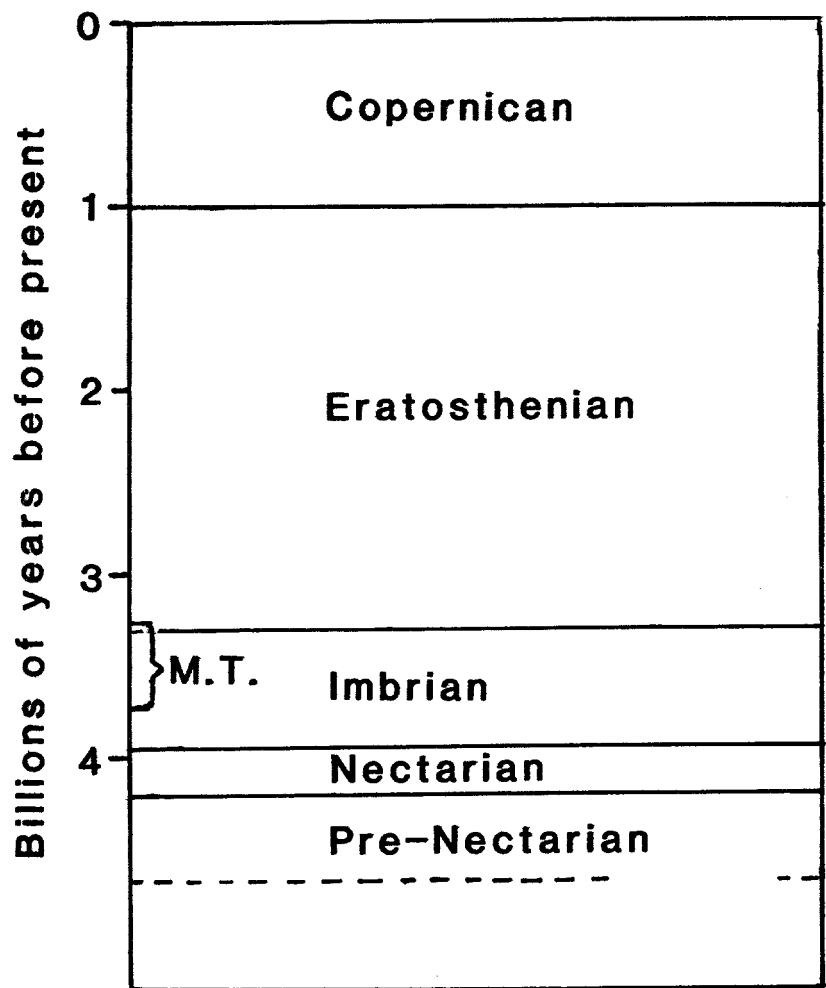


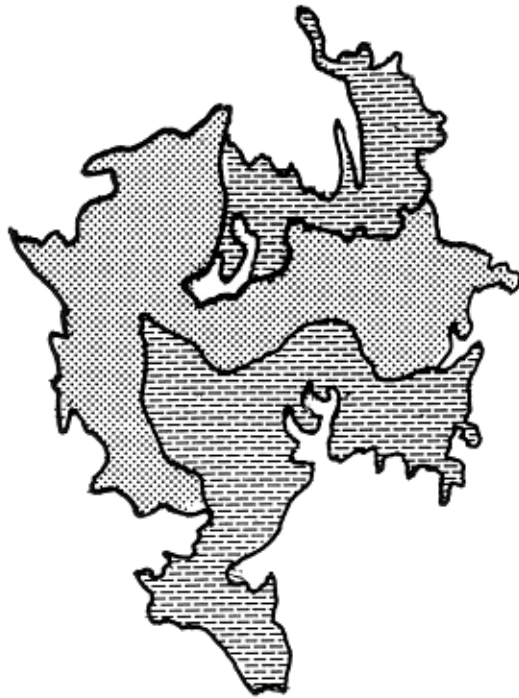
Fig. 2. Lunar time scale.

Wilhelms (1987, p. 235) states that "Mare Tranquillitatis contains northern and southern belts of the intermediate-age group (i.e., Im-2) of Upper Imbrian basalt, separated by a belt of the young age group (i.e., Im-3)." This description does not match the distribution of the two units as shown on the maps of the Julius Caesar and Taruntius quadrangles. No belt of Im-3 is shown on the Julius Caesar quadrangle. No belts appear on the Taruntius quadrangle. There is further confusion in that neither quadrangle map matches the distribution of spectral units shown on Wilhelms' Plate 4A (Fig. 3a) or the distribution of age groups of basalts shown on Plate 9A (Fig. 3b). Unit Im-1 is found largely, but not entirely, along the margins of the mare. On the Julius Caesar quadrangle (Morris and Wilhelms, 1967), which covers most of the western part of the mare, Im-2 is shown as the most widespread unit, but on the Taruntius quadrangle (Wilhelms, 1972), which covers much of the northeastern part of the mare, the most widespread unit is Im-3. Unfortunately, along the common border of the two quadrangles, the boundaries between the two units do not match. The mismatch evidently reflects differences in interpretation of unit boundaries. Finally, Plates 4A and 9A do not completely reflect variations in color shown in the color difference photograph of E.A. Whitaker (Fig. 4).

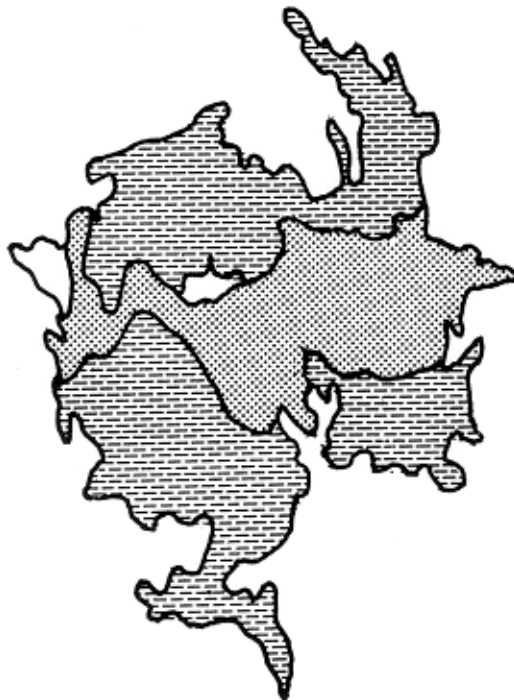
The differences between distribution of units shown on Plates 4A and 9A and distribution as shown on photogeologic maps are probably due to the fact that the maps were prepared before data from remote sensing became available. Those data obviously were used in preparing Plates 4A and 9A. It is now recognized that reflectance of lunar materials is more a function of composition than of age.

Pre-mare Features

The floor of the basin over which the mare materials were erupted was highly irregular. The margins of the mare, therefore, are also irregular. The basalt flows were not thick, and in places islands of the floor rocks appear in the mare (Figs. 5 and 6). They are strikingly developed along the north and east sides of Tranquillitatis. Furthermore, certain ridges mapped on the mare appear to be related to irregularities in the floor. The most conspicuous example is Lamont (Fig. 5), a ringlike ridge that is 70 km in maximum diameter and lies NNW of the Apollo landing site. This



a) Spectral classes of basalts:
 stippled-HDWA (high-Ti basalts);
 lined-complex or unknown.



b) Age groups:
 Stippled-youngest basalts;
 Lined-basalts of intermediate age.

Fig. 3. Basalts in Mare Tranquillitatis, based on Wilhelms (1987), plates 4A and 9A.



Fig. 4. Color difference photograph of the near side of the Moon, made by subtracting a photograph taken at $0.31 \mu\text{m}$ from one taken at $0.61 \mu\text{m}$. Courtesy of E.A. Whitaker.

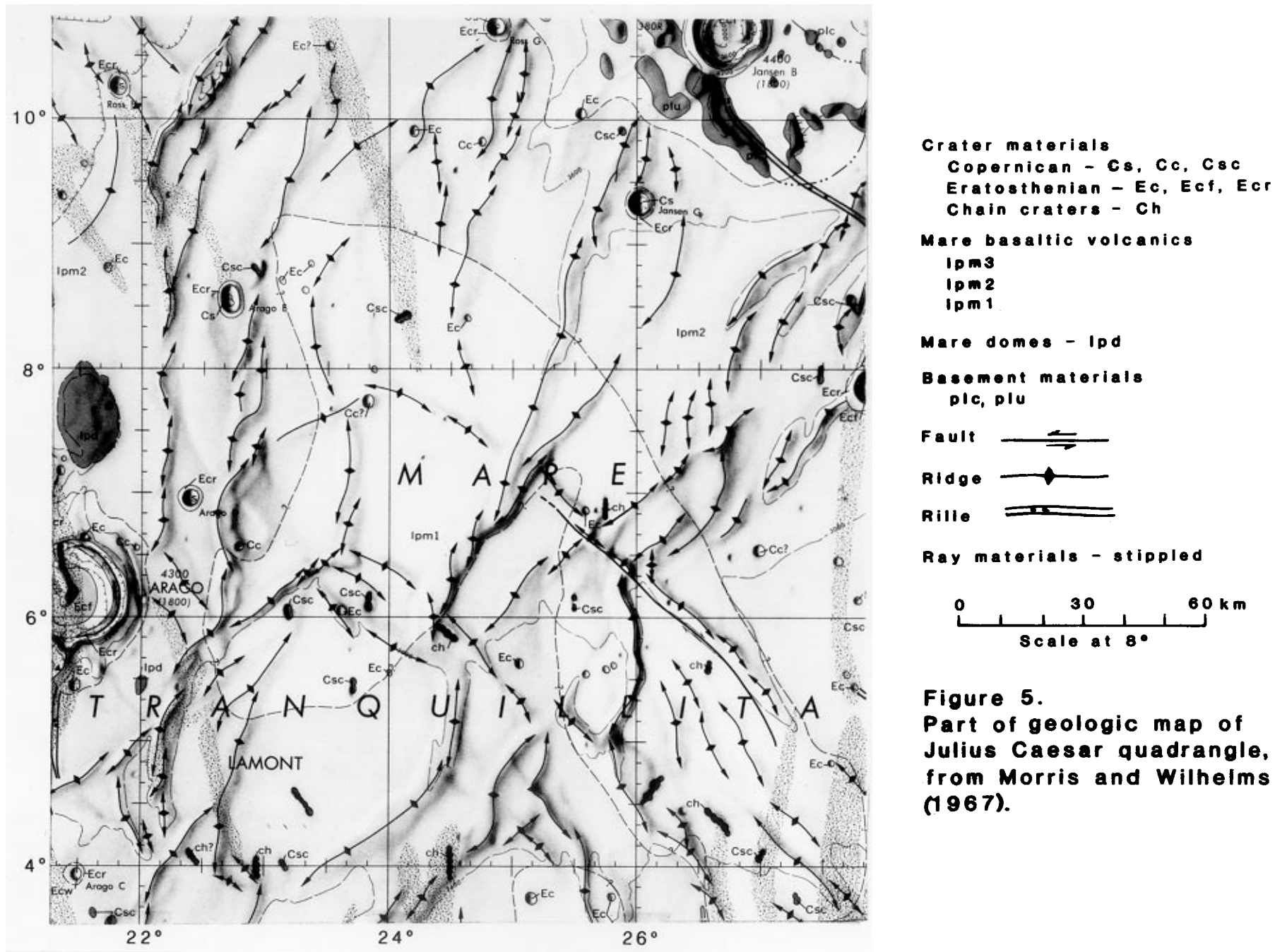
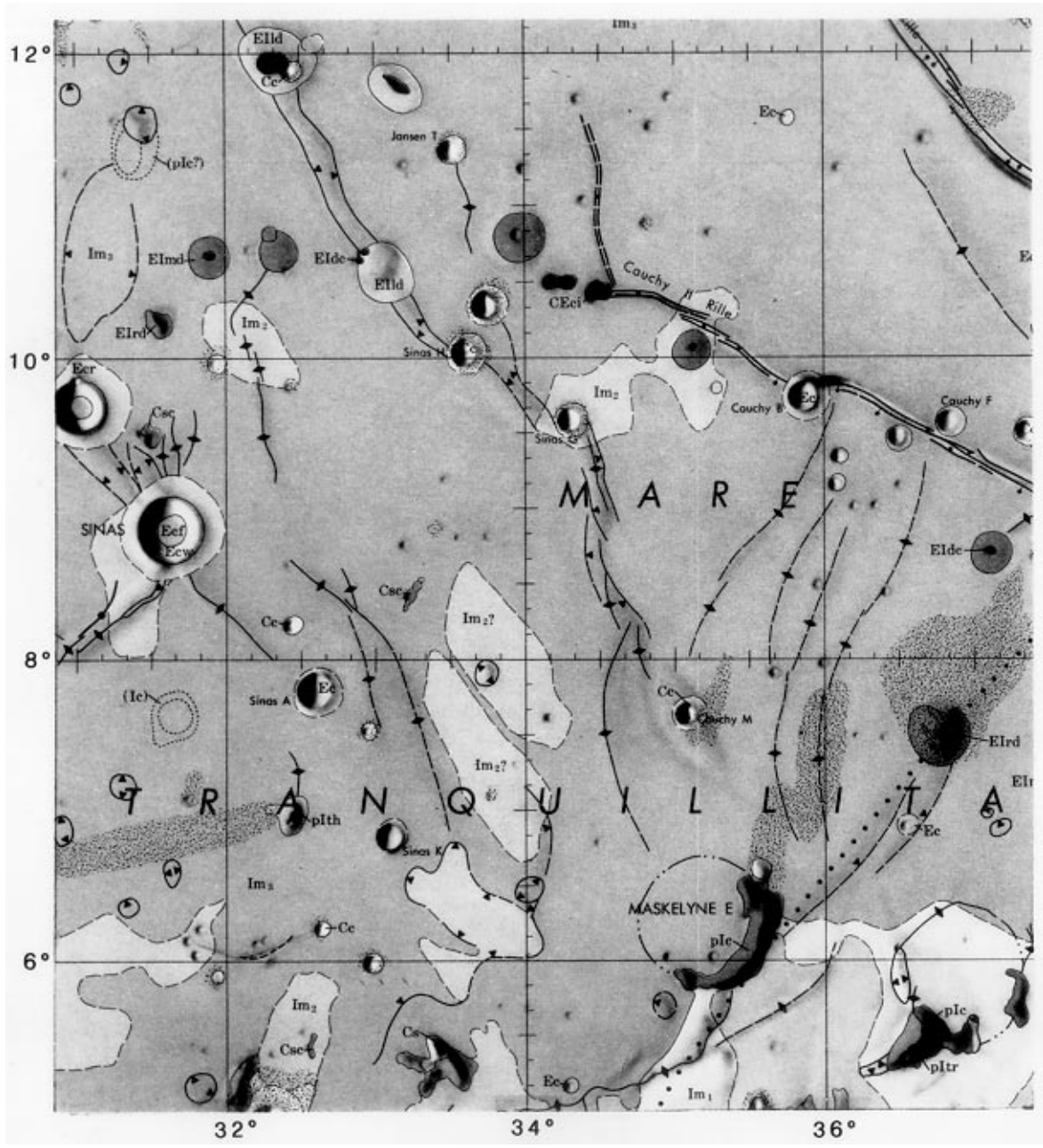


Fig. 5. Part of geologic map of Julius Caesar quadrangle from Morris and Wilhelms (1967).

6



Crater materials
 Copernican - Cs, Cc, Csc
 Copernican or Eratosthenian - CEci
 Eratosthenian - Ec, Ecr, Ecf, Ecw

Mare basaltic materials
 Im₃
 Im₂
 Im₁

Mare volcanic domes -
 Elmd, Elld, Eldc, Elrd

Basement materials
 plc, pltr, plth

Ridge —◆—

Scarp —▼—

Barb points downslope

Possible mare dome ○

Rille ———

Ray materials - stippled



Figure 6.
Part of geologic map of
Taruntius quadrangle, from
Wilhelms (1972).

Fig. 6. Part of geologic map of Taruntius quadrangle from Wilhelms (1972).

has been interpreted as a ridge formed by settling of mare material over the rim of a large pre-mare crater. There are similar, less well developed features elsewhere on the mare. There are also pre-mare craters that are only partly buried by mare material (e.g., Maskelyne E, on Fig. 6).

Mare Features

General Statement

Much of the surface of Tranquillitatis is apparently a gently undulating surface, but there are a number of features that disturb the surface and must be considered in selecting mining sites. The most important are ridges, rilles, basement islands, domes, and craters with associated ejecta blankets. Rays are an additional feature discussed below.

Ridges

Ridges 1 to 5 km in width and a few km to more than 100 km in length are a common feature of Tranquillitatis, especially in the western and northwestern parts. They range from straight to arcuate to sinuous. The characteristics of mare ridges have been summarized by Wilhelms (1987, pp. 107-110) from studies by numerous investigators. Ridges range from a few to tens of kilometers in length and from 2 to 10 km in width. A central spine is a common feature, superposed on the rounded arch-like profile of the typical ridge. A ridge may be bounded by a scarp or a narrow graben on one side. Ridge heights of up to 100 meters appear to be indicated.

Rilles

Rilles are graben, straight or curved, that appear to be related to subsidence along fractures. The rilles are narrow troughs with flat floors up to a few kilometers wide and steep walls 50 to 250 m high. Rilles on Tranquillitatis range from tens of kilometers to more than 300 kilometers in length. They are most numerous in the western part of Tranquillitatis, but the Couchy I and Couchy II rilles of the eastern part of the mare (Fig. 6) are respectively 275 and 210 km in length.

Domes

Domes are rounded structures, circular to elliptical in plan, that are a few to 25 km in maximum diameter. They are considered to be volcanic structures superimposed on the mare basalts. As indicated below, their total area is only a very small fraction of the area of the mare.

Basement Islands

Basement islands occur mostly close to the margins of the mare. They are parts of the floor that were too high to be covered by the floods of mare basalt.

Craters

Craters and their ejecta blankets are undoubtedly the most important obstacle to mining on Mare Tranquillitatis. Craters are present throughout the mare. Craters visible on the geologic maps and the Orbiter II medium and high-resolution photographs used in the present study range from 44 km in diameter (Plinius) down to 2 m, the lower limit of resolution. Shoemaker and others (1967) showed that the number of craters per unit area of the mare increases exponentially with decrease in diameter, and this relation is apparent in any plot of diameter versus numbers of craters. Figure 7 is an example from the present study.

Impacts of bodies of a wide range of sizes have been producing craters on Tranquillitatis ever since eruption of the mare volcanics about 3.6 b. y. ago. In general, the characteristics of the craters are a function of their age. High-resolution photographs show a complete range from the sharp, fresh-appearing Copernican craters to older craters (very late Imbrian to Eratosthenian) that have been virtually obliterated and now appear as shallow depressions with faint rims and gently-sloping walls (Fig. 8); they are barely recognizable as craters. Such craters show no bright halos and no blocks either inside the craters or on their rims.

The impact craters of the Moon are known to be of two genetic types, primary and secondary. Primary craters are those produced by impacts of bodies arriving on the moon from space. Secondary craters are those produced by impacts of material ejected from the primary craters. In some cases the two can be distinguished; more often they cannot. Distinction between the two types has not been attempted in the present study.

Ejecta Blankets

Ejecta blankets consist of materials thrown out of impact craters, traveling along ballistic trajectories. There is a progression from coarsest materials at or close to crater rims to finest materials farthest from the rims. The halo of debris produced by impact may be symmetrical if the

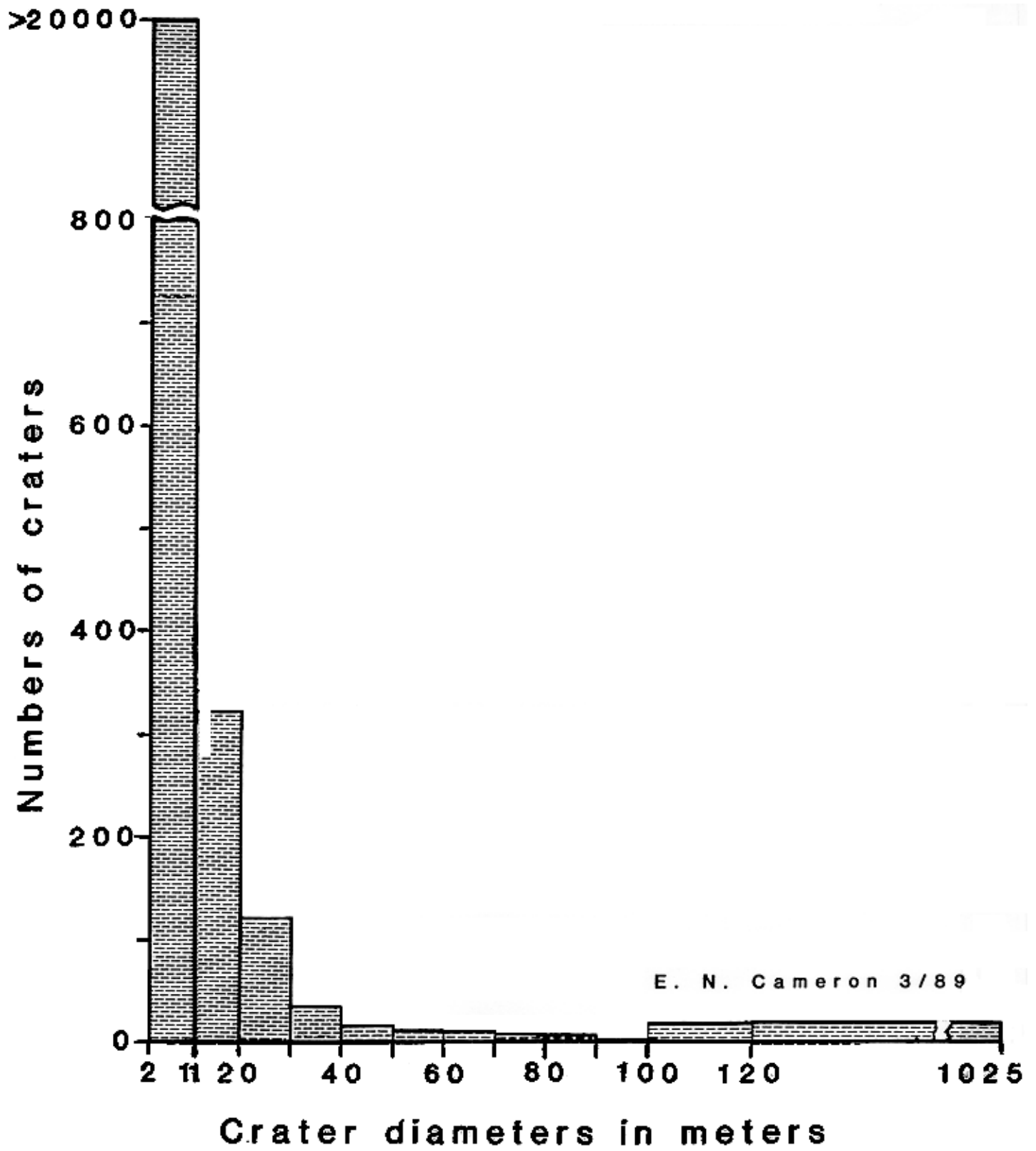


Fig. 7. Mare Tranquillitatis, Lunar Orbiter photograph II-84H₁, numbers of craters in relation to size.

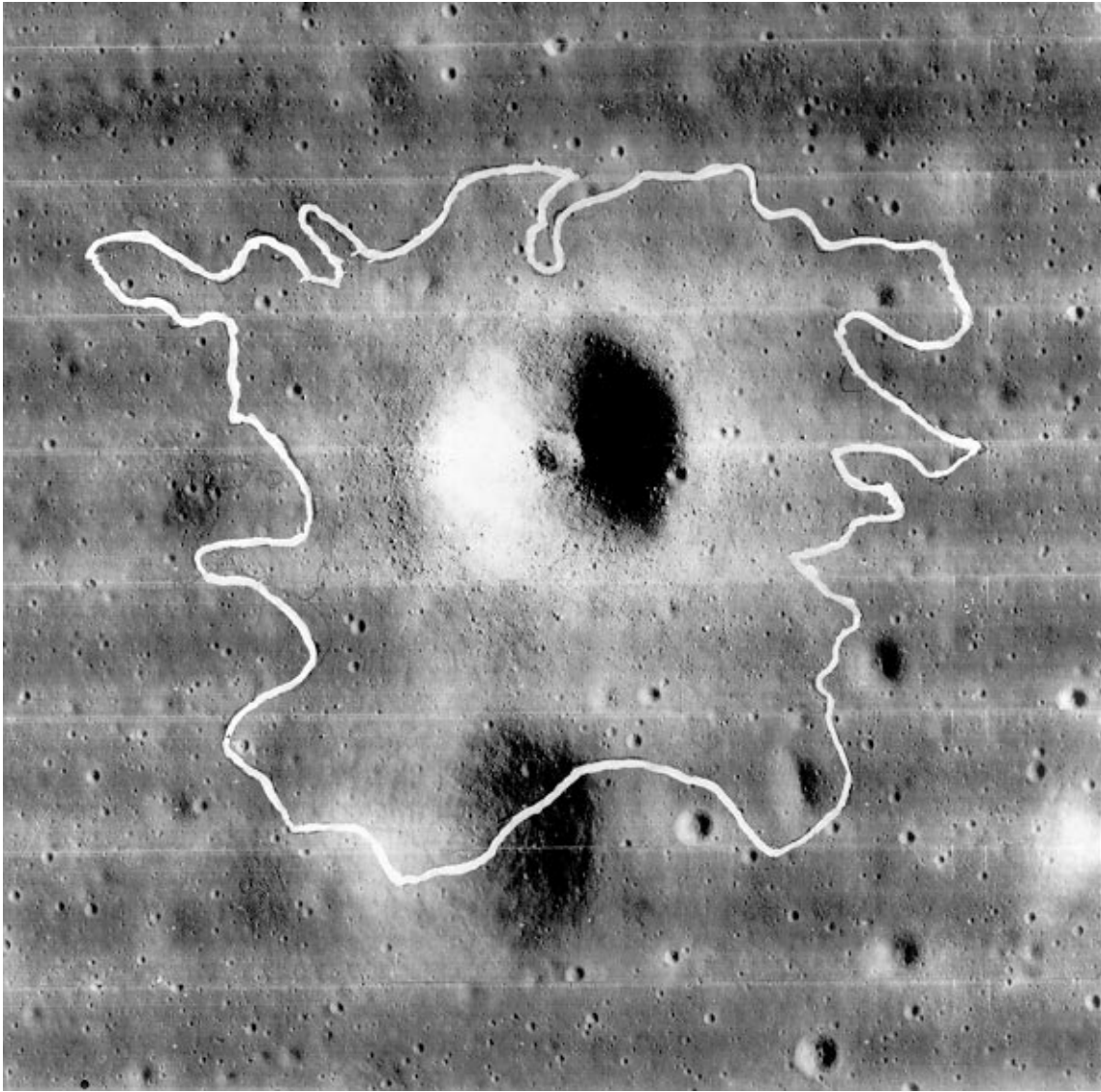


Fig.8. Copernican crater, 440 m in diameter, on Lunar Orbiter photograph II-83H₃. Ejecta blocks 2 m or more in diameter are shown over the area bounded by the white line.

missile path is perpendicular to the surface or nearly so, but the halo will become asymmetrical as the angle of incidence is increased. Figure 8 shows an example of an irregular ejecta halo around a Copernican crater. The white line shows the limit beyond which blocks greater than 2 m in diameter (the resolution limit of the photograph) are not present. Since for each Orbiter photograph the angle of incidence of sunlight is given, depths of newer craters can be calculated from the widths of shadows of the walls and the measured diameters of the craters. As indicated in Fig. 9, ratios for newer craters vary but are mostly close to 0.25. With an average depth of regolith of 3 m, bedrock blocks are to be expected in regolith around craters greater than about 12 m in diameter. Around older craters, however, ejecta blocks may have been partly or even totally destroyed by later impacts.

Ray Materials

Rays are streams of ejecta produced by impacts upon the moon. They fall into two groups. The first consists of rays that are associated with certain Copernican craters on the mare and are recognizable on photographs owing to their brightness. They extend outward 1 to 7 crater radii from the rims of craters. The second group consists of elongate to irregular areas of material; the patches range up to 85 km in length and 20 km in width. They are scattered widely over Tranquillitatis. They are considered to be thin blankets of ejecta from major craters that are mostly outside the mare. Many of those on Tranquillitatis are attributed to the crater Theophilus, about 360 km south of the Apollo 11 landing site, and ray materials are most extensive in the southwestern part of Tranquillitatis, which lies directly north of Theophilus. Ray materials of this type are poorly indicated on photographs used in the present study. The ray areas delineated on geologic maps have been plotted on the basis of telescopic observations from Earth. There appears to be little information about the composition or texture of the ray materials, other than the fact that blocks are not visible in them on high-resolution photographs, so that any blocks present in ray materials must be less than 2 m in diameter. Highland material is likely to be present in the more extensive rays, hence they must be considered as sources of dilution of mare-derived regolith. To what extent rays will prove to be unminable, owing either to dilution or the presence of blocks, is

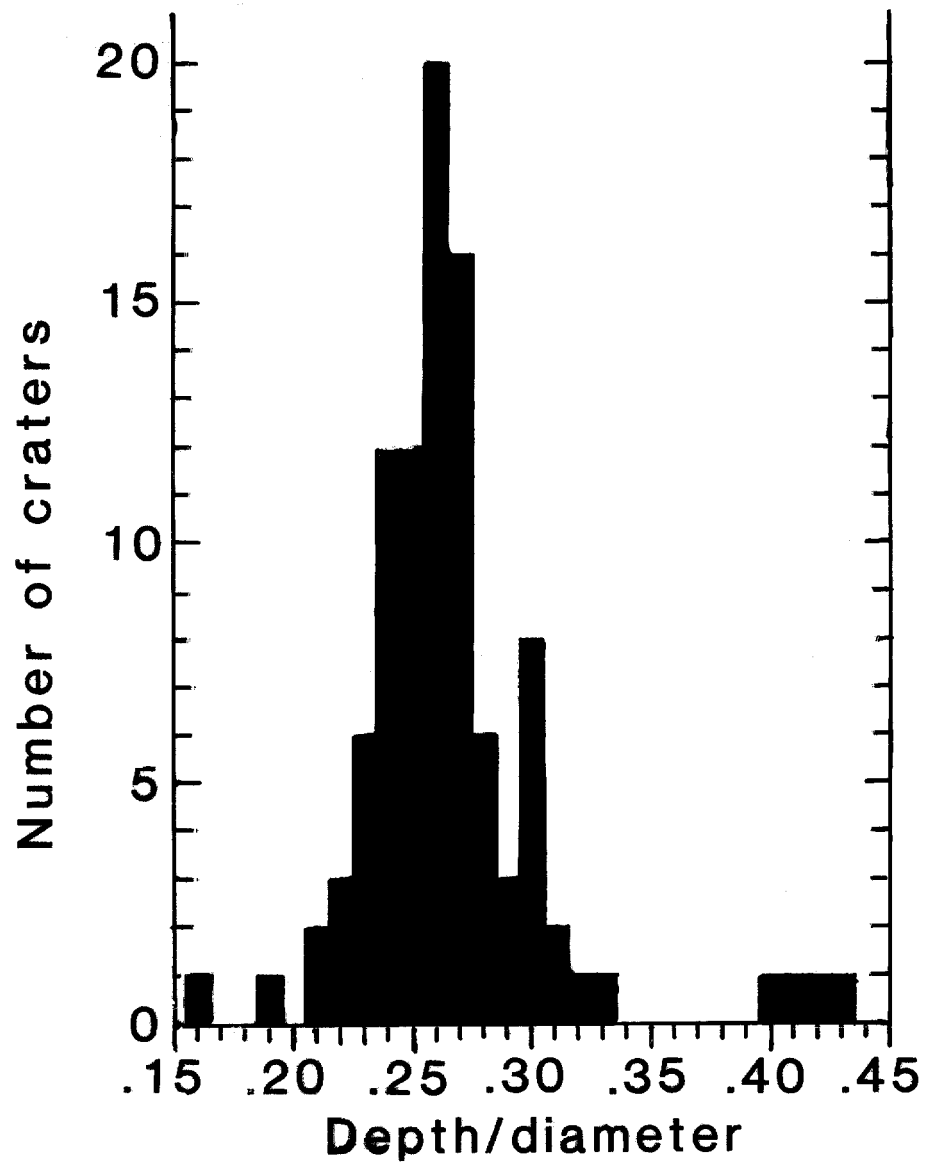


Fig. 9. Depth/diameter ratios of 98 craters, as determined from Lunar Orbiter photograph II-84H (prints H₁, H₂, H₃).

uncertain. However, the Apollo 12 landing site on a ray from the great crater Copernicus suggests that blocks will not be a significant factor.

The Mare Regolith

General Description

Lunar regoliths have been the subject of numerous studies, beginning with the pioneering work by Shoemaker and others (1967). The name is applied to the loose, predominantly fine-grained material that blankets the lunar surface. The regolith has two major components, (1) particles of minerals and rocks and (2) agglutinates. Agglutinates are mineral and rock particles welded together by glass produced by partial melting of rock and mineral material due to impacts. In the early stage of formation, a regolith consists of a high proportion of mineral and rock fragments. As gardening of the regolith by impact continues, the proportion of agglutinates rises, finally reaching a stage at which the number of particles produced by comminution is balanced by the number of agglutinate particles formed. At this point the regolith is said to be mature. In general, the regolith of an ancient mare like Tranquillitatis will be mature. However, there will be variations in maturity where recent impacts have brought new materials to the surface.

Mare regoliths are derived mainly from the immediately underlying basaltic volcanics, but they are contaminated, perhaps everywhere, by highland material ejected from large post-mare craters in adjacent highlands and also from intra-mare craters that penetrate to the floor of the mare. Thus Papike and others (1982) point out that whereas mare basalts from Apollo 11 and Apollo 17 contain 10.5 to 13.5% TiO_2 , the overlying regoliths contain only 7.5 to 8.5% TiO_2 . They attribute the difference to contamination with highland material, clearly indicated by the appearance of highland material in the modal analyses discussed below.

Modal Composition

The modal composition of the regolith at the Apollo 11 site has not been completely determined, but the composition of the 90-20 μm fraction is given in Table 1, and the composition of the 1,000-90 μm fraction is given in Table 2. Lithic fragments and fused components are not included in Table 1.

Table 1

Grain Count Modal Data for the 90-20 μm Fraction of Apollo 11 Sample 10084 (Papike and Others, 1982)

| | |
|----------------|-------|
| Plagioclase | 21.4% |
| Pyroxene | 44.9 |
| Olivine | 2.1 |
| Silica | 0.7 |
| Ilmenite | 6.5 |
| Mare glass | 16.0 |
| Highland glass | 8.3 |
| TOTAL | 99.9% |

Table 2

Grain Count Modal Data for the 1000-90 μm Fraction of Sample 10084 (Papike and Others, 1982)

| | |
|----------------------|-------|
| Lithic fragments | |
| Mare basalt | 24.0% |
| Highland component | 2.3 |
| Fused soil component | 59.5 |
| Mineral fragments | |
| Mafic | 4.2 |
| Plagioclase | 1.9 |
| Opaque | 1.1 |
| Glass fragments | 4.5 |
| Devitrified glass | 1.8 |
| Other | 0.3 |
| TOTAL | 99.9% |

Grain (Particle) Size

Samples of the regolith brought back by Apollo 11 consist predominantly of particles less than 1 mm in diameter (Table 3). It should be noted, however, that no large bulk samples were obtained, and there is no information on the abundance of large blocks; such blocks would certainly not be included in the samples.

Table 3

**Grain Size Distribution in Apollo 11 Sample 10084,853
(from Criswell and Waldron, 1982)**

| <u>Size Fraction</u> | <u>Wt. %</u> | <u>Cumulative Wt. %</u> |
|---------------------------|--------------|-------------------------|
| 4-10 mm | 1.67 | 1.67 |
| 2-4 mm | 2.39 | 4.06 |
| 1-2 mm | 3.20 | 7.26 |
| 0.5-1 mm | 4.01 | 11.27 |
| 250 μm -0.5 mm | 7.72 | 18.99 |
| 150-250 μm | 8.23 | 27.22 |
| 90-150 μm | 11.51 | 38.72 |
| 75-90 μm | 4.01 | 42.73 |
| 45-75 μm | 12.40 | 55.14 |
| 20-45 μm | 18.02 | 73.15 |
| -20 μm | 26.85 | 100.00 |

The only appraisal of particle size distribution in total regolith that I have been able to find is that of Shoemaker and Morris (1968). Those investigators made a detailed study of particle size distribution in regolith as displayed in high-resolution photographs taken at the Surveyor I, III, V, VI, and VII sites. Resolution of the photographs is 1 mm, hence only particles 1 mm and larger could be counted. Size-frequency curves were plotted for these particles and extrapolated to sizes smaller than 1 mm (Fig. 10). The curves indicate the predominance of particles less than 1 mm

in diameter in the regolith. Surveyor I landed inside Crater Flamsteed, but Surveyor III, Surveyor V, and Surveyor VI landed on typical maria, respectively Oceanus Procellarum, Mare Tranquillitatis, and Sinus Medii. Larger particles include both solid rock fragments derived from bedrock and agglutinates of varying cohesion. It seems likely (H. Schmitt, personal communication) that many of the latter will be disintegrated during excavation and handling on a mining machine.

Structure of the Regolith

The structure of the regolith, in the few core samples brought back by the Apollo missions, has been studied in detail. A crude, mostly indistinct layering is generally present. It is inferred from this that the regolith consists predominantly of successive and interleaved ejecta blankets spread out around the craters. A typical blanket must originally have consisted of a more or less circular sheet thinning away from its inner edge at the crater rim. Given the range of impact magnitudes, widths of ejecta halos must range from millimeters to kilometers, and thicknesses of halos at their inner edges must range up to tens of meters or more. Once formed, an ejecta halo becomes subject to modification, interruption, or even partial or complete obliteration by later impacts. As a result, it must be expected that the internal structure of the regolith will be extremely complex. The implications of this for exploration of the regolith will be discussed in a later report.

Thickness of the Regolith

The thickness of the regolith on Tranquillitatis is a matter of prime importance for the mining of helium and is a controlling factor for all estimates of tonnage of regolith available. The thickness will certainly vary from place to place. Thickness should be nil or nearly nil on the rims and floors of very young craters. Thickness should be greatest just outside the rims, then decrease progressively with distance from the rims. The same rules, however, should not apply to very old craters, which have undergone long periods of degradation due to gravitational slumping and continued bombardment. There may be very little variation in thickness of regolith across them.

There are no direct measurements of regolith thickness on the surface of Tranquillitatis. Estimates of thickness are based on studies of craters and ejecta as displayed on lunar photographs,

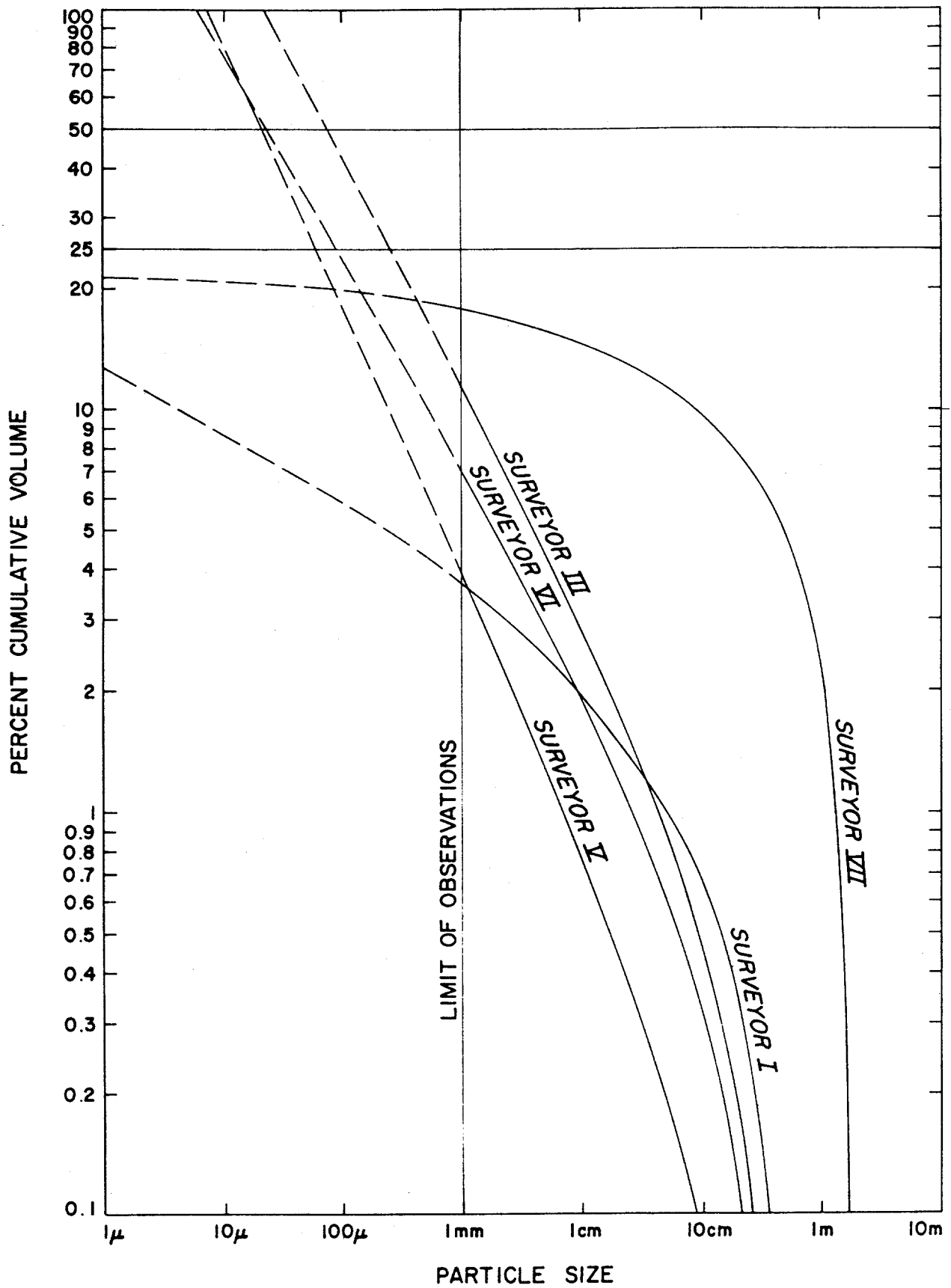


Fig. 10. Volumetric particle size-frequency distributions of particles of the lunar regolith 1 mm or more in diameter for 50% porosity. Dashed lines are extrapolations for smaller particles. From Shoemaker and Morris (1968).

mathematical modeling of the mechanics of crater formation (Melosh, 1975), and passive seismic experiments. Shoemaker and others (1967) noted at the Surveyor V landing site that two craters respectively 15 m and 20 m in diameter were surrounded by strewn fields of blocks. Assuming crater depth to diameter ratios of between 1/3 and 1/5, they concluded that the depth of regolith is not greater than 5 meters. Shoemaker and others (1970) estimated regolith thickness at the Apollo 11 landing site at 3 to 6 m. This estimate is based on the observed depths of anomalous flat-floored craters and craters with central mounds, assuming that the floors are at the top of the bedrock surface. Nakamura and others (1975), from the passive seismic experiment, calculated the depth of regolith at the Apollo 11 site as 4.4 m.

The writer believes that information on the thickness of the regolith over broad areas is best obtained at present from studies of very small craters on high-resolution photographs of the mare. A special study of such craters on high-resolution photographs of the area east of the Apollo 11 landing site has therefore been made. Findings of the study are the following:

1. All craters less than 12 m in diameter (the smallest visible are 2 m in diameter) are fresh craters with sharp rims. Presumably they are of Copernican age.
2. Many such craters are superimposed on older larger craters with less distinct rims.
3. The density of fresh craters, as indicated by counts of sample areas, is in the neighborhood of 1,000 per sq. km.
4. Depth-diameter ratios of most small fresh craters are very close to 0.25 (Fig. 9). This holds for small craters away from larger craters as well as for those superimposed on older craters.
5. Fresh craters less than 18 m in diameter have smooth walls and floors. No blocks or other irregularities are visible within them. Bedrock was evidently not penetrated by the craters.

From these observations the following conclusions can be drawn:

1. By the time the young, fresh craters began to be formed, older craters less than about 4.5 m deep (less than 18 m in diameter) had been obliterated by impacts.
2. By early Copernican time the regolith was already more than 3 m deep.

3. An estimate of 3 m for the average depth of regolith away from larger craters is therefore conservative, especially in view of the presence of regolith more than 3 m deep on the rims of older craters.

In a subsequent section, an average depth of regolith of 3 m and a ratio of depth to diameter of 0.25 is used as the basis for delineating block-strewn areas around craters; i.e., areas of regolith containing blocks of bedrock.

Helium Content of the Regolith

Information on the helium content of the regolith of Mare Tranquillitatis is from two sources: (1) analyses of samples taken from the Apollo 11 landing site and (2) inferences based on the relationship between the He contents and the TiO₂ contents of lunar regoliths in general. Helium contents of various Apollo 11 samples are given in Table 4. The data are for bulk samples and for "breccias", particles produced by impact-welding of regolith particles. Note that the average He content of breccias is higher than the average He content of the fines, despite the fact that analyses of size fractions invariably show that He is enriched in the finest fractions (Fig. 11), whereas the breccia particles are much coarser. No explanation of this anomaly is at hand.

There are four problems in using analyses of Apollo 11 regolith samples for evaluation of helium resources. The first problem is whether the regolith at the Apollo 11 landing site is representative of the regolith of the surrounding mare. According to Wilhelms (1987, p. 235), the lunar module Eagle was about 400 m west of the 180-m-wide, 30-m-deep crater "West" between blocky rays of the crater, and Beaty and Albee (1978, 1980) suggested that almost all the samples were derived from the ejecta of the crater. Exposure ages of samples indicate the crater is about 10⁸ years old. At the landing site, bedrock-derived finer ejecta between the blocky rays may thus have covered, or at least contaminated, the normal regolith of the mare, which may be higher in He content due to greater age and longer exposure to the solar wind.

The second problem is possible loss of helium from regolith during excavation and handling of the materials before analysis. Hintenberger and others (1970) analyzed two sets of grain-size fractions of Apollo 11 regolith sample 10084. Mass balance calculations show that for one set

Table 4
Helium-4 Contents of Apollo 11 Samples

A. Regolith Samples

| <u>Sample</u> | <u>He-4 wppm</u> | <u>Reference</u> |
|---------------------|----------------------|-------------------------------|
| 10010 | 20 | Funkhouser and others, 1970 |
| 10010 | 34 | |
| 10084,18, fines | 34 | Hintenberger and others, 1970 |
| 10084, 18, fines | 37 | Hintenberger and others, 1971 |
| 10084,8, fines | 34 | |
| 10084,40, fines (1) | 44 | Funkhouser and others, 1970 |
| 10084,40, fines (2) | 41 | |
| 10084,29, fines (1) | 40 | Marti and others, 1970 |
| 10084,48, fines (1) | 35 | Pepin and others, 1970 |
| 10084,48, fines (2) | 40 | |
| 10084,40, fines (3) | 40 | |

B. Breccia Samples

| | | |
|----------|----|-------------------------------|
| 10021,20 | 67 | Hintenberger and others, 1975 |
| 10046,16 | 36 | |
| 10048,27 | 56 | |
| 10060,24 | 58 | |
| 10061,11 | 58 | |
| 10061,33 | 60 | |
| 10018 | 43 | |
| 10021 | 67 | |
| 10023 | 45 | |
| 10027 | 27 | |
| 10048 | 38 | |
| 10061 | 85 | |
| 10068 | 45 | |

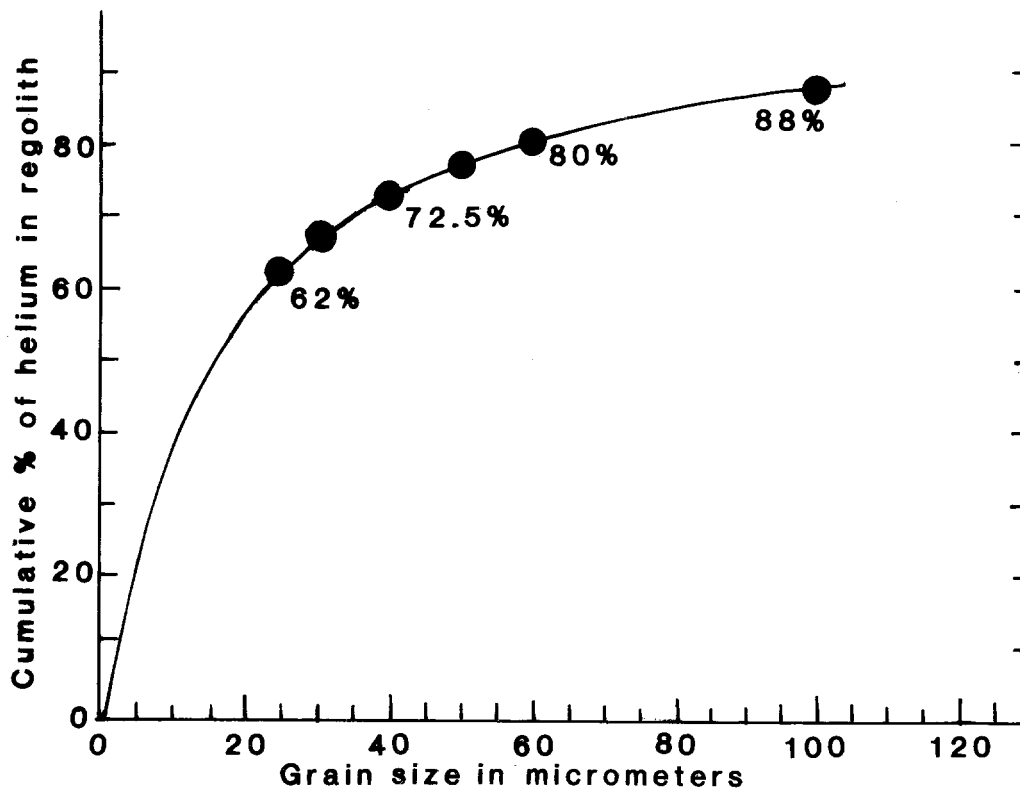


Fig. 11. Percentage of total helium in relation to grain size in Apollo 11 regolith sample 10084, based on data from Criswell and Waldron (1982) and Hintenberger and others (1970).

total helium content of the fractions is 22% less than the content reported for the bulk sample. For the second set the deficiency is 31%. Analytical error is given as only 3%, and nothing in the article suggests a source of such large discrepancies. Similar deficiencies for samples from Apollo 16 and Apollo 17 have been noted by Swindle and others (1990). The size fractions were obtained by sieving, and one must suppose that He was lost during the mechanical handling involved. This leads one to question whether there was further loss during excavation of the samples and handling prior to the arrival of the samples at the analytical laboratory. If so, the He contents reported for regolith samples may be a better index of how much He will actually be present at the heating stage of the extraction process, after excavation and processing of the regolith, than of the He content of regolith in the ground. Further investigation is clearly needed to resolve this problem.

The third problem is that all samples of regolith returned from the Apollo 11 site are surface samples, hence there is no direct information on variation in the He content of the regolith of Mare Tranquillitatis with depth. However, samples from drill holes at the Apollo 15, Apollo 16, and Apollo 17 sites are relevant here, since they suggest what variations in He content with depth may be expected in lunar regoliths. Results of analyses of cores from drill holes at the three sites are given in Table 5. The Apollo 15 and Apollo 16 cores show variation in He content but no correlation of content with depth. The average He content of the Apollo 15 samples is 10.8 wppm. The average for 11 Apollo 15 surface samples is 11.1 wppm. The average for Apollo 16 core samples is 6.4 wppm. The average for 22 surface samples (Hintenberger and Weber, 1973; Haskin and others, 1973; Walton and others, 1973) is 6.7 wppm. The Apollo 17 drill core shows an increase in He content with depth. Apollo 17 samples are too heterogeneous to permit calculation of a meaningful average He content. At any rate, core and surface samples give no indication of a systematic decline, or increase, in the He content of regolith with depth. This is hardly surprising. Given the repeated overturn of regolith due to impact gardening during the more than 3 billion years since Mare Tranquillitatis was formed, no systematic pattern of variation with depth is likely to be found. Instead, an irregular pattern of small-scale variation, both vertically and laterally, is to be expected. For any given site, the range of helium content in depth could well be the same as that shown by surface samples.

The fourth problem is that samples from the Apollo 11 landing site provide the only direct evidence of the He content of the regolith of Mare Tranquillitatis. The He content of the regolith of the mare as a whole must be inferred from data for lunar regoliths in general. For mare regoliths, the following findings (Cameron, 1988, 1990) are critical to the delineation of areas of regolith that are enriched in He:

- (1) Regoliths of some maria or parts of maria contain less than 20 wppm He, but regoliths of certain other maria have He contents ranging from 25 to nearly 50 wppm.

Table 5
Helium-4 in Apollo 15, Apollo 16, and Apollo 17 Cores

Apollo 15*

| <u>Sample</u> | <u>Depth cm</u> | <u>He-4 wppm</u> |
|---------------|---------------------|----------------------|
| 15001 | 149 | 15 |
| | 154 | 11 |
| | 160 | 13 |
| | 163 | 12 |
| | 168 | 12 |
| | 176 | 9 |
| | 187 | 6 |
| | 206 | 7 |
| 15003 | 217 | 13 |
| | 220 | 14 |
| | 226 | 9 |
| | 231 | 13 |
| | 238 | 10 |
| | 242 | 10 |
| | 246 | 9 |
| | 253 | 11 |

Apollo 16**

| <u>Sample</u> | <u>He-4 wppm</u> |
|-----------------------|----------------------|
| 60007 (top barrel) | 4-7 |
| 60006 | 5-7 |
| 60004 | 8-9 |
| 60003 | 6-8 |
| 60001 (bottom barrel) | 4 |

Data for 5 of 7 core barrels representing depths of about 13 cm to about 200 cm.

Apollo 17+

| <u>Sample</u> | <u>Depth cm</u> | <u>He-4 wppm</u> |
|-------------------|---------------------|----------------------|
| 70008,163,284 | | 8 |
| 70008,205,228/283 | | 9 |
| 70008,15,285 | | 13 |
| 70006,10` | | 13 |
| -----140----- | | |
| 70005,10 | | 23 |
| 70004,10 | | 21 |
| 70003,10 | | 20 |
| -----240----- | | |
| 70002,10 | | 17 |
| 70001,10 | | 21 |
| -----290----- | | |

*Hübner and others, 1973. **Heymann and others, 1978. +Pepin and others, 1975.

- (2) The helium content of a regolith sample is primarily a function of its composition and its exposure time; i.e., the time over which it has been exposed to the solar wind. As to composition, the TiO₂ content is particularly important (Cameron, 1988). Analyses of lunar samples show that in general regolith samples enriched in TiO₂ are likewise enriched in He (Fig. 12). The relationship is not perfect, and the scatter in the diagram is undoubtedly due in considerable part to difference in the exposure times of the various samples. At present the most useful index of exposure time is the maturity index, defined as I/TiO₂, where I is the intensity of the ferromagnetic resonance of the sample. Jordan (1989) has shown that a more linear relationship is obtained if the He content is plotted against (I/FeO) TiO₂. However, means of measuring the maturity index by remote sensing are still not worked out, hence the He/TiO₂ relationship is still the best available index of the He content of regolith. It is so used in this report.

MINABLE AREAS IN MARE TRANQUILLITATIS

General Statement

There are three major questions to be answered in determining the minability of regolith in Mare Tranquillitatis:

- (1) What percentage of the total area of the mare is covered by high-TiO₂ regolith, and what variations in He content within high-TiO₂ areas are to be expected?
- (2) How much of the total area of the mare, roughly 300,000 sq. km, is physically amenable to mining for He-3?
- (3) What is the distribution and what are the sizes of the minable areas?

Pending further investigation of the mare, no final answers to these questions can be given. The following sections, however, summarize available relevant information and provide preliminary answers.

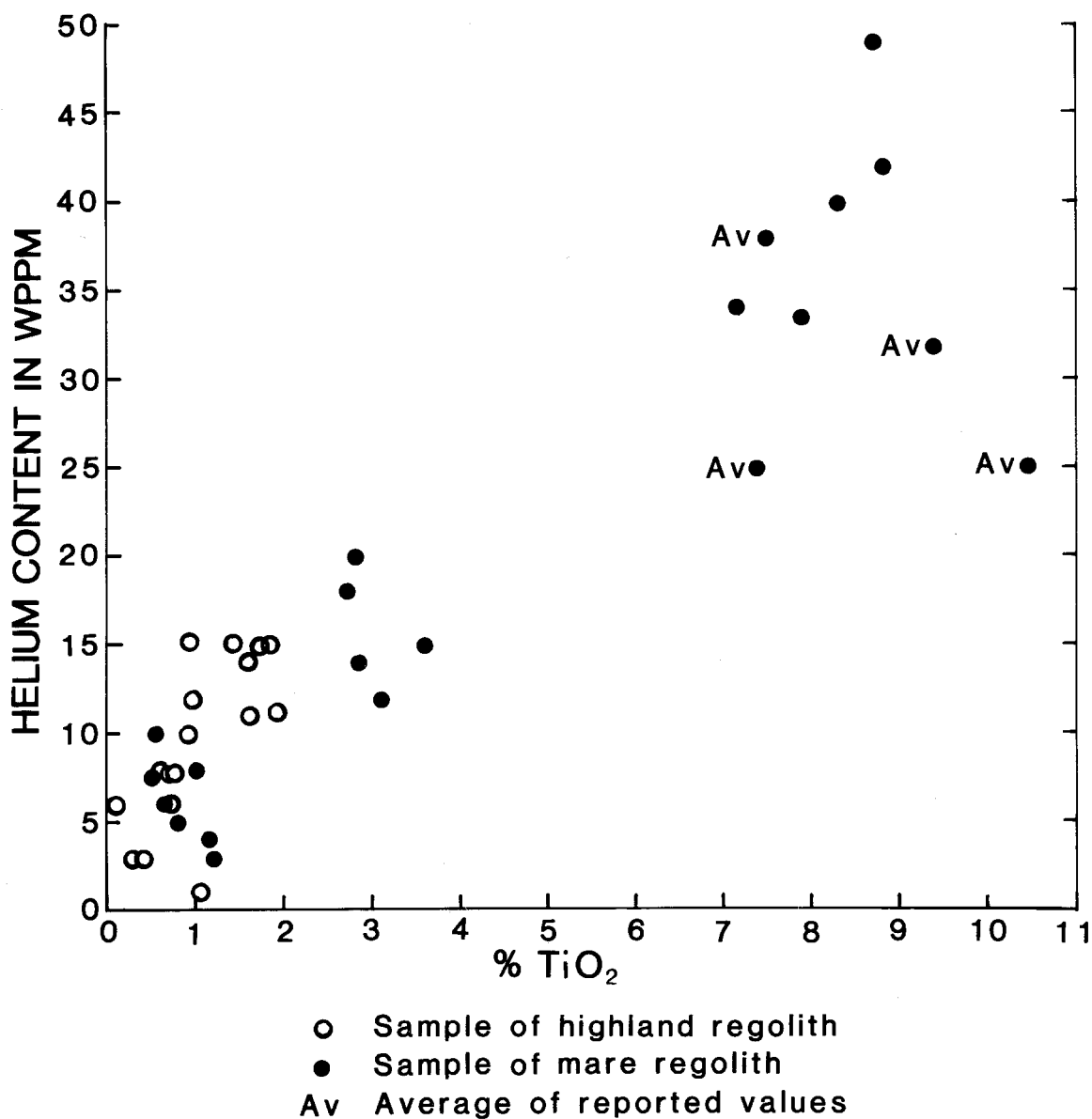


Fig.12. Relation between He contents and TiO₂ contents of lunar regolith samples. Data from Bogard and Hirsch (1978), Bogard and Nyquist (1972), Criswell and Waldron (1982), Cuttitta and others (1971), Cuttitta and others (1973), Eberhardt and others (1970), Eberhardt and others (1972), Eugster and others (1975), Funkhauser and others (1970), Haskin and others (1973), Heymann and Yaniv (1970), Heymann and others (1972a, 1972b), Heymann and others (1973), Heymann and others (1978), Hintenberger and others (1970), Hintenberger and others (1971), Hintenberger and others (1974), Hintenberger and Weber (1973), Hintenberger and others (1975), Hubner and others (1973), Hubner and others (1975), Kirsten and others (1972), Laul and others (1974), Laul and Papike (1980), Laul and Schmitt (1973), Ma and others (1978), Marti and others (1970), Nava (1974), Pepin and others (1970), Pieters and others (1980), Pieters and McCord (1976), Rose and others (1974), Wilhelms (1987), Willis and others (1972). From Cameron (1988).

Percentage of the Mare Occupied by High-TiO₂ Regolith

As indicated in my previous report (Cameron, 1988), information on the distribution of high-TiO₂ regolith in Mare Tranquillitatis, apart from the Surveyor V and Apollo 11 sites, is entirely from remote sensing. In the original version of the present report, data from remote sensing were used to classify the regolith of Tranquillitatis into three categories. The distribution of the three categories was plotted in the diagram of Fig. 15. At the time the diagram was prepared, the most informative material available consisted of the color difference photograph by E.A. Whitaker (Fig. 4) which covers the entire mare, and the spectral ratio map of Johnson and others (Fig. 13), which covers all but the northeastern part. Figure 4 covers the entire mare, whereas Fig. 13 does not include the northeastern part. For the parts covered by both, agreement is good, if we take into account that in Fig. 13 all high-Ti regolith is lumped into a single category of +6% TiO₂. Areas in the category 3 to 6% TiO₂ correspond closely to the brightest areas in Fig. 4. However, on Fig. 4 the remainder of the mare shows as black areas interspersed with areas that are mottled with various shades of dark to medium gray. The only interpretation of the pattern possible at present is that the spectrum of grays reflects variations in the TiO₂ content of regolith within the area shown on Fig. 13 as having +6% TiO₂. If the lower limit is slightly more than 6%, then the upper limit is about 7.5%. This is the content of Apollo 11 regolith; Apollo 11 landed on a black area or on an area that is black finely mottled with dark gray.

On an overlay of an enlargement of the portion of Whitaker's photograph that covers Mare Tranquillitatis (Fig. 14) the areas occupied respectively by black regolith, dark to medium gray regolith, and light gray regolith were outlined. The result is Fig. 15. Calculations from measurements made on Fig. 15 indicate that 28% of the mare is covered by black regolith in part mottled with dark gray, 65% by dark gray to medium gray regolith, and 7% by light gray to white regolith. The inferred TiO₂ contents of the three classes are respectively 7.5%, 6 to 7.5%, and 3 to 6%. The black regolith should then contain 30 to perhaps 45 wppm of He, the dark to medium regolith presumably will contain 20 to 30 wppm He.

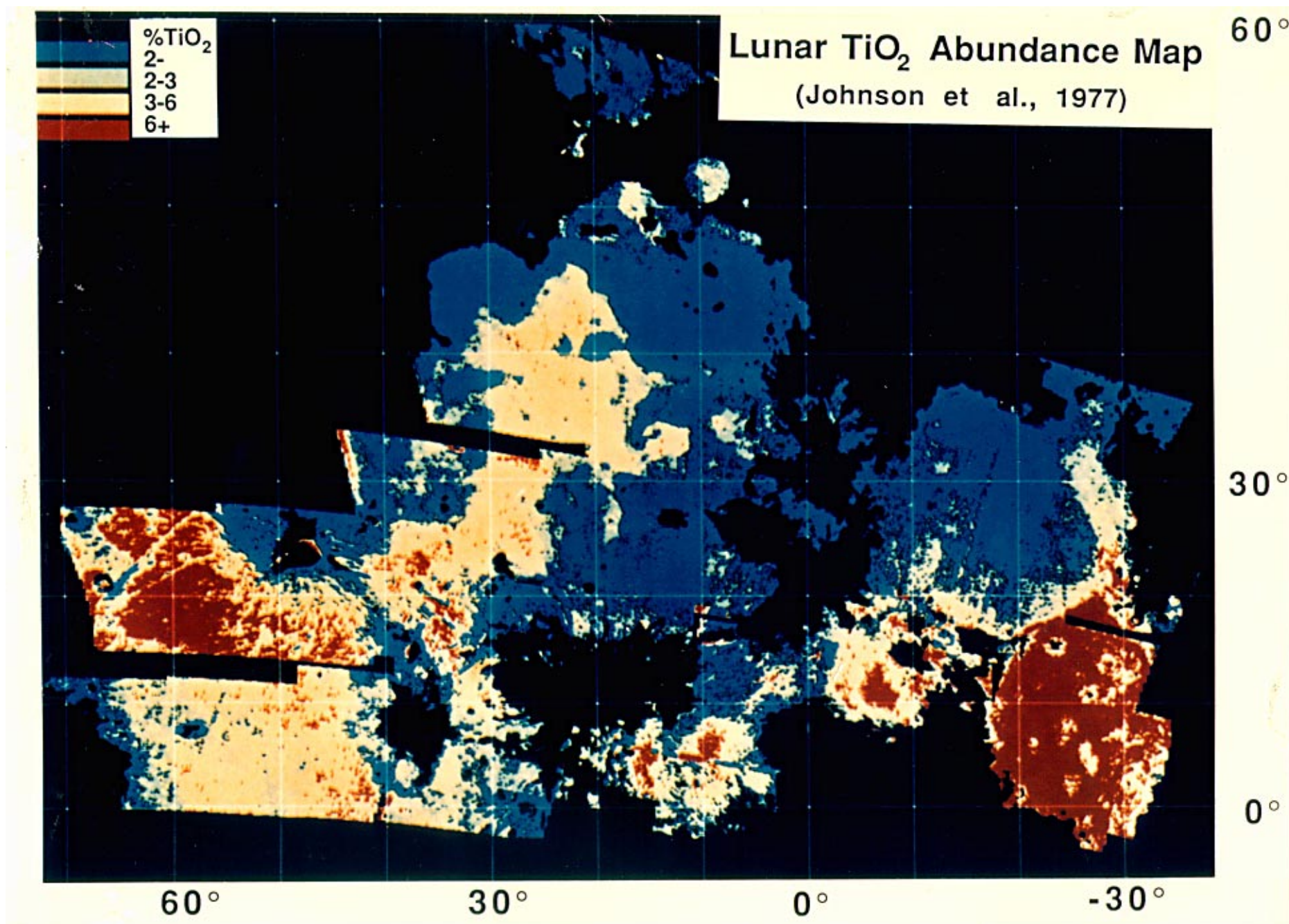


Fig. 13. Lunar TiO₂ abundance map, using the 0.38/0.56 μm ratio. From Johnson et al. (1977).

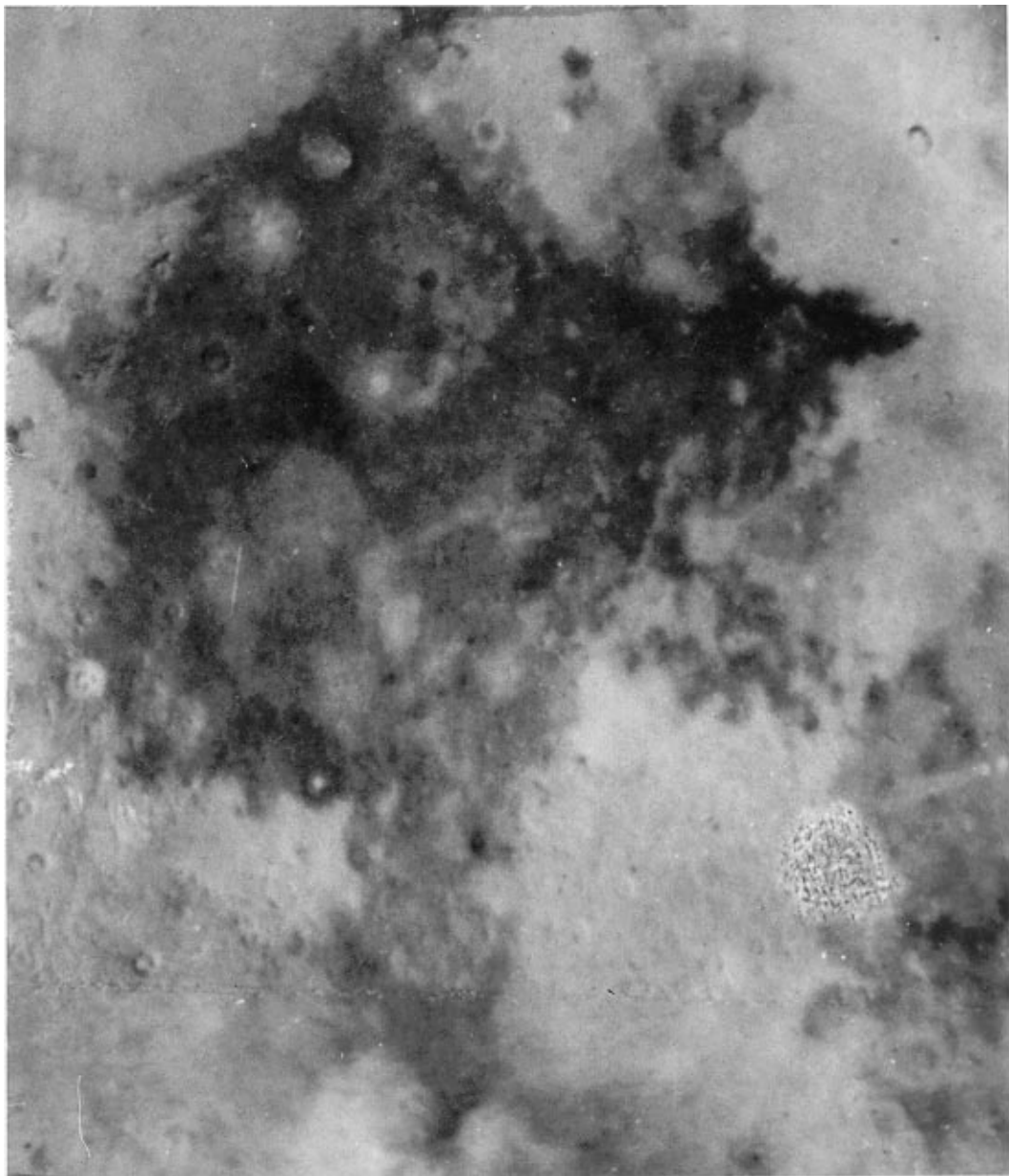


Fig. 14. Enlargement of Mare Tranquillitatis from Fig. 4.

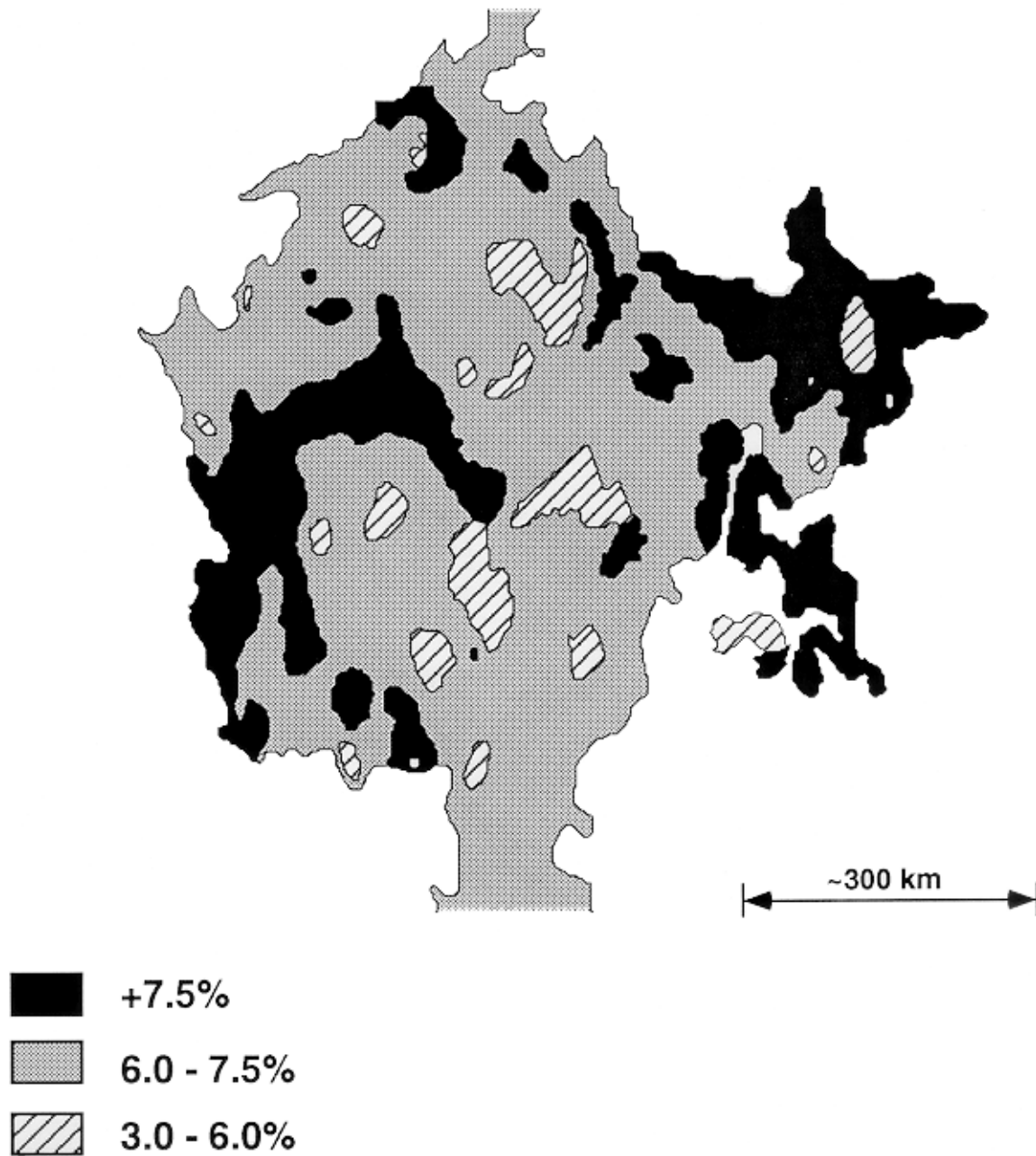


Fig. 15. Inferred variations in TiO₂ content of regolith of Mare Tranquillitatis. Based on photograph by E.A. Whitaker (1965), and spectral ratio TiO₂ abundance map by Johnson et al. (1977).

The estimates of helium content apply to mature regolith. As discussed earlier, maturity is a function of length of exposure to the solar wind. Given the nature of the process of gardening of the regolith by impacts, exposure time may vary both laterally and vertically in the mare. Such variations cannot be detected by any of the available methods of remote sensing. However, Apollo 11 regolith samples are mature, and given the great age of Mare Tranquillitatis and the evidence that successive generations of craters have been created and then destroyed or largely destroyed by impacts, it seems reasonable to infer that much of the mare is underlain by mature regolith. Besides maturity, degree of dilution with highland material will also affect the helium content. Only systematic sampling can determine actual patterns and degree of variation.

Since my report of 1990 was written, J.R. Johnson and others (1991) have published a TiO₂ abundance map of the lunar nearside constructed from 0.40/0.56 μm ratio values converted to weight percent TiO₂ using the calibration curve of Fig. 16, in which TiO₂ is plotted against measured 0.40/0.56 μm values divided by 0.40/0.56 μm ratio values for the MS-2 region of Mare Serenitatis. The ratio images for mare areas are classified into 9 units, <3%, plus 8 units from 3 to 10+%. On their abundance map high-TiO₂ regolith (6% or more TiO₂) in Mare Tranquillitatis is largely confined to the western half of the mare. The TiO₂ content of the regolith of most of the eastern half of the mare is shown as 4 to 5%, but there are small patches with <3% TiO₂ and other small patches with 6% TiO₂.

Besides the TiO₂ abundance map of the entire lunar nearside, Johnson and others produced two enlarged abundance maps of west central Mare Tranquillitatis with a resolution (pixel size) of 1.2 km. On the western half of one of the maps (their Figure 7, upper map) a large area with 6% to more than 10% TiO₂ is shown.* This map was used as the base for a sketch map outlining the region of TiO₂ abundance of 7% or more on a part of the geologic map of the Julius Caesar quadrangle. I have enlarged this map to the scale of the original geologic map and have plotted on

*In a report on further work at the University of Arizona on TiO₂ abundances, Melendrez (1992) reports that isolated regions containing regolith with about 15% TiO₂ have been identified in western Tranquillitatis.

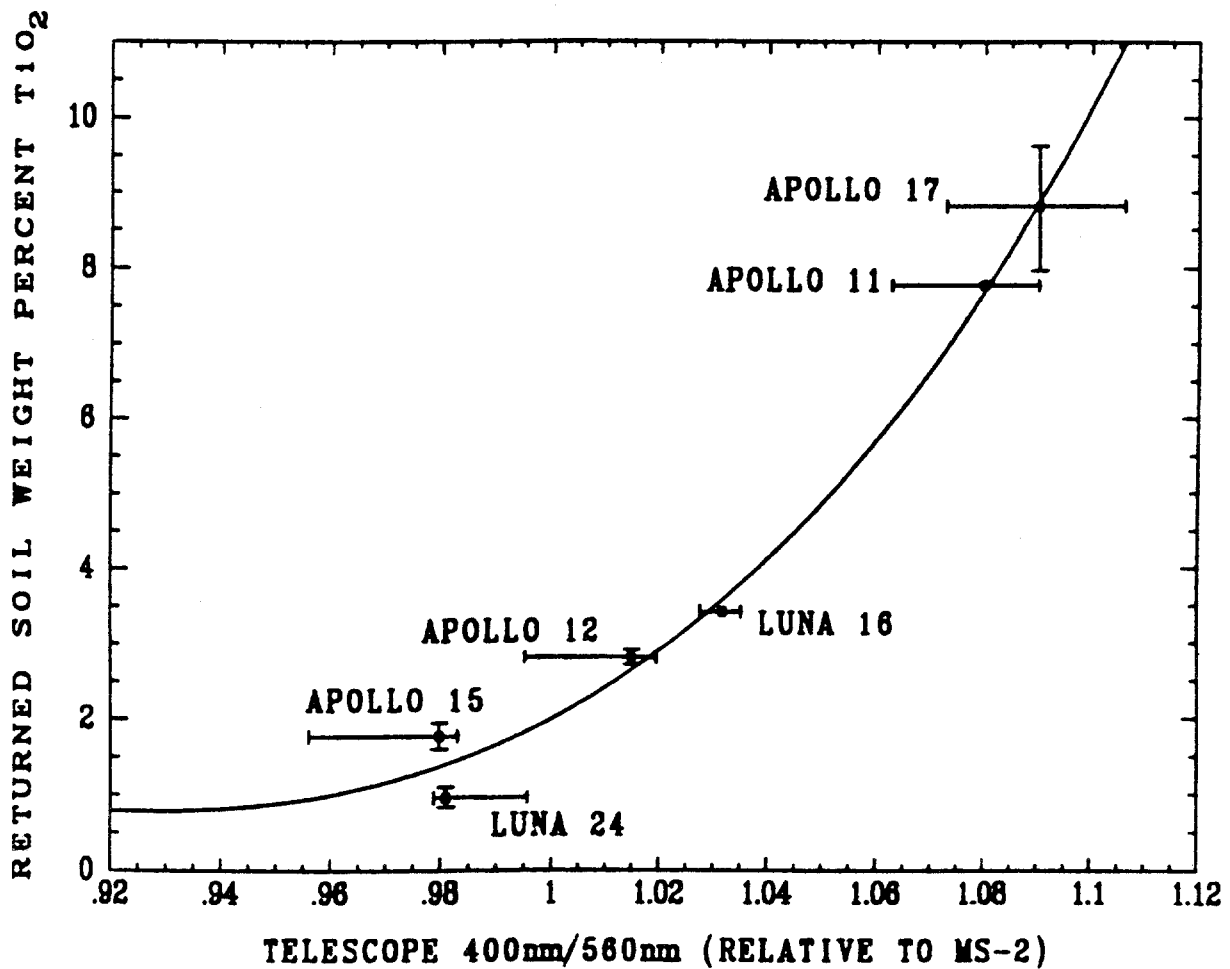


Fig. 16. Empirical calibration of telescopic 0.40/0.56 μm ratio values divided by the 0.40/0.56 μm ratio value for MS-2 to weight percent TiO_2 . MS-2 is the standard region in Mare Serenitatis. From Johnson and others (1991).

it the boundary of category A regolith (+7.5% TiO_2) from an enlargement of Fig. 15 to the same scale. The result is Fig. 17.

Considering the sources of error in reflectance maps and in interpreting the color difference photograph of Whitaker (Fig. 4), agreement of the two high-Ti boundaries is reasonably good. Sources of error in measuring and interpreting spectral ratios are discussed in detail by Johnson and others, the most serious being errors in measurement of spectral ratios (± 2 wt.% for values above 3% TiO_2) and inadequate calibration of the curve of Fig. 16 in the range above 3% TiO_2 . The accuracy of the earlier spectral ratio map by Johnson and others (1977) is estimated by them at

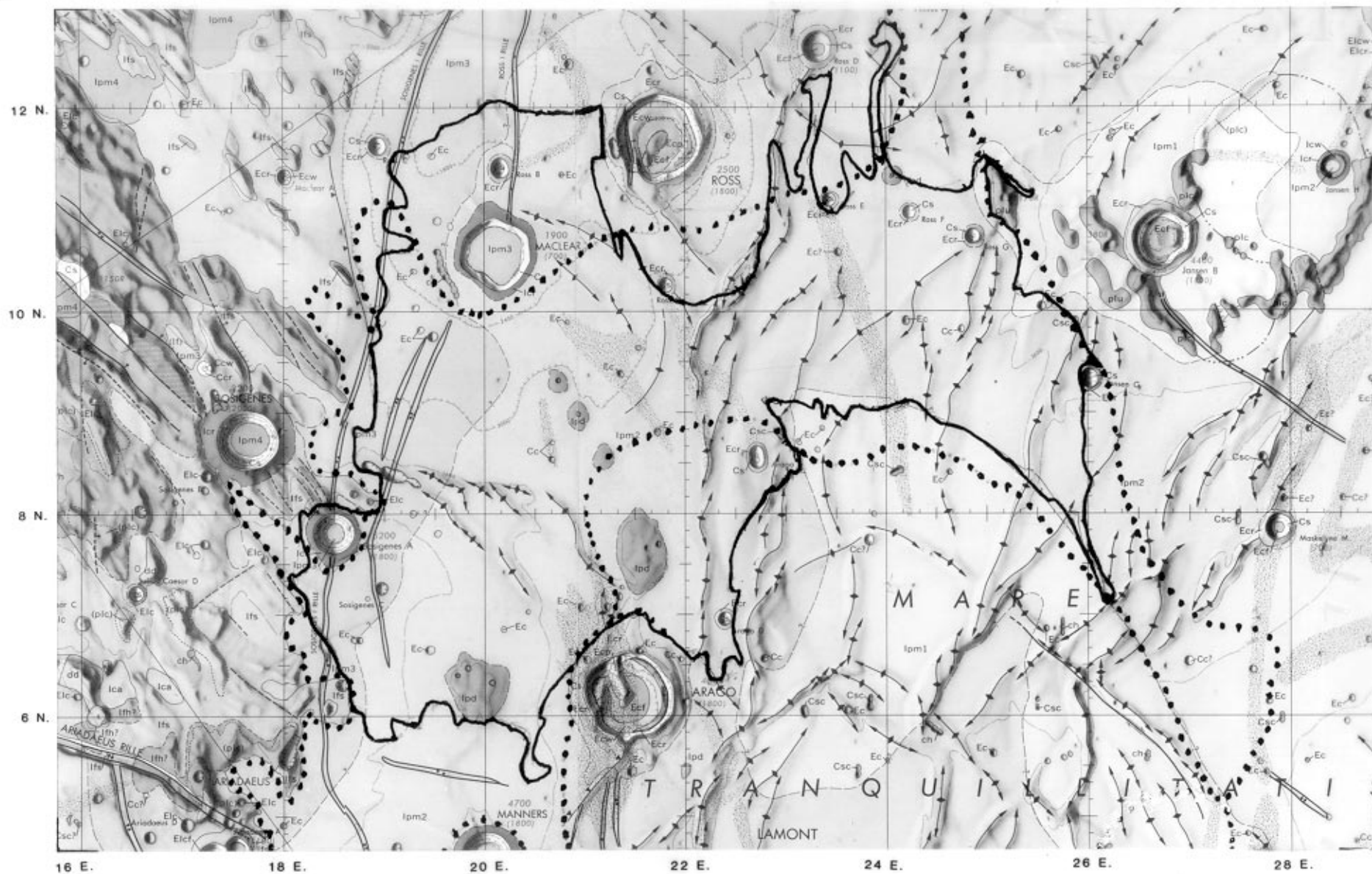


Fig. 17. Part of the Julius Caesar quadrangle on which Johnson and others (1991) plotted the boundary (heavy solid black line) of the region of TiO₂ abundances of 7 wt. % or more. Superimposed on this is the boundary (heavy dotted line) of regolith with 7.5 wt. % or more TiO₂ from Fig. 15.

± 2 wt.% for values above 5 wt.% TiO_2 and $<1\%$ for values below 4 wt.% TiO_2 . Differences in the spectral ratios used in the three studies cited here may be a factor. In the study of the Whitaker photograph, there is certainly a subjective factor involved in assigning various mottled areas to one category or another in Fig. 15.

Both Fig. 15 and the map of the lunar nearside by Johnson and others (1991) show an area of high- TiO_2 regolith extending along the western side of Tranquillitatis southward from the south boundary of Fig. 17 into the Apollo 11 area. For the east central and eastern part of the mare, however, agreement is poor. The enlargement of the Whitaker photograph (Fig. 14) shows sizable areas that are black or black mottled with dark gray. These are indistinguishable from the high- TiO_2 areas in the western part of the mare and were therefore interpreted as high- TiO_2 areas in preparing Fig. 15. The interpretation is consistent with the map of Johnson and others (1977). In contrast, these areas are shown on the map by Johnson and others (1991) mostly as regolith with TiO_2 contents ranging from 3 to 6%.

At present there is no satisfactory explanation of these discrepancies. Part of the difficulty is deciding what is being measured in reflectance studies. The problem is apparent from studies of high-resolution photographs of the Apollo 11 and Ranger VIII areas. These have a resolution of 2 m. The resolution (pixel size) of the spectral ratio map of Fig. 13 is 3 km, whereas the resolution of the enlarged TiO_2 abundance map of western Tranquillitatis by Johnson and others (1991) is 1.2 km. On Fig. 18, which shows a typical high-resolution photograph of a portion of the area east of the Apollo 11 landing site and includes the area of Fig. 8, a 1.2 km square is plotted. No matter where this square is placed on the photograph, it will cover a variety of craters ranging from those that are still sharp-rimmed and obviously very young to those that are in an advanced stage of obliteration. Around the young craters, even the smallest ones, there are bright ejecta halos, for which UV/VIS ratios must be relatively low. Around the old craters there are no such halos; UV/VIS ratios must be relatively high and the same as those for the surrounding regolith. Exposure times (hence maturity) of regolith will vary widely over any 1.2 km square

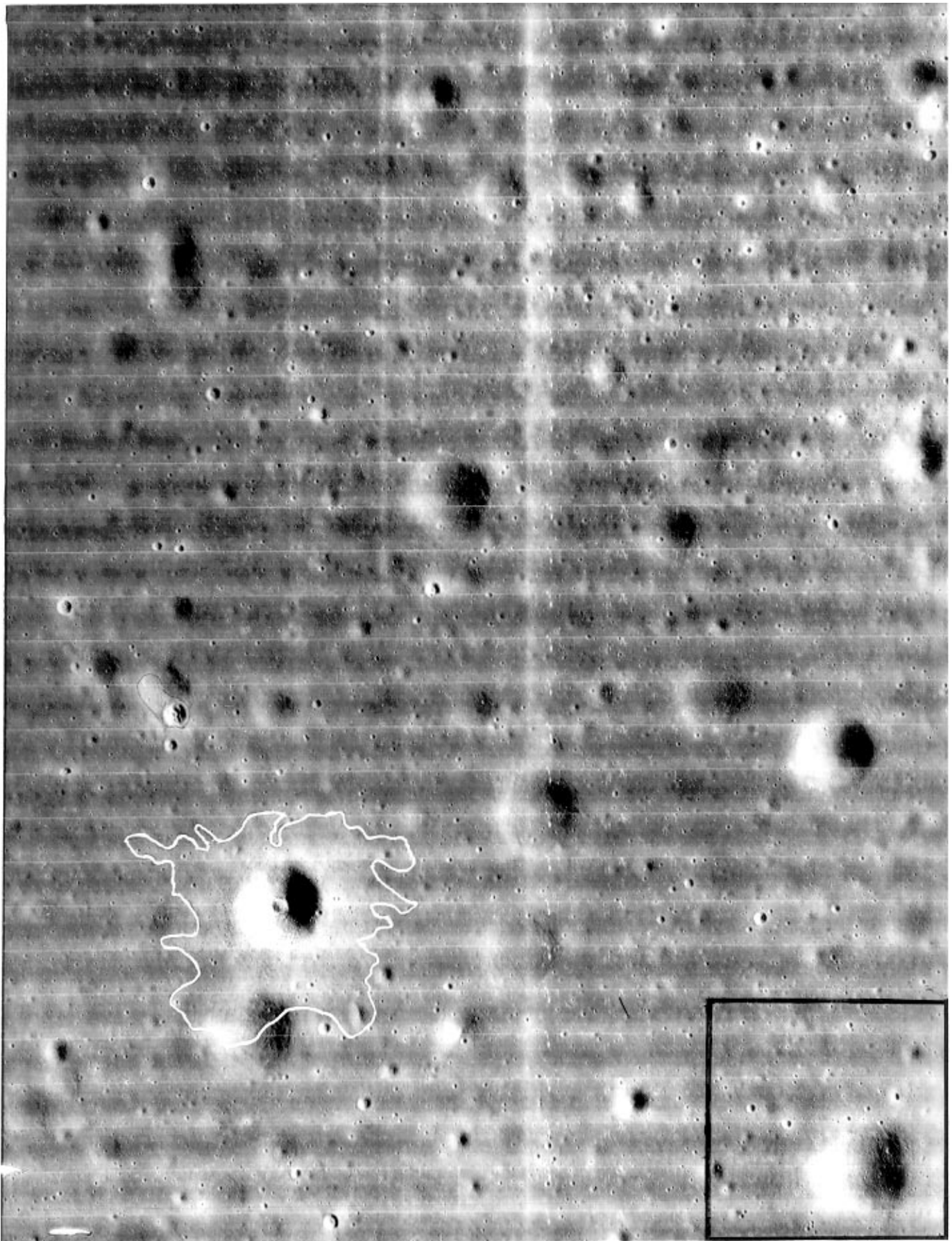


Fig. 18. Lunar Orbiter photograph II-83 H₃, reduced from the original size of 40 × 90 cm. The box outlined in black in the lower right corner is 1.2 km square. Figure 8 is an enlargement of a portion of the photograph.

area. Measurement of such an area will inevitably give an average value of a range of reflectance ratios that are not determined solely by variations in the TiO_2 content of regolith. This has now been recognized by the investigators at Arizona on the basis of reflectance measurements with improved resolution (Melendrez, 1992).

Another matter that must be considered in interpreting reflectance ratios is the nature of mining operations involved in recovering He and other gases from the regolith. The ejecta halos around younger craters that have penetrated bedrock will contain blocks of rock that must be separated from the regolith before it can be treated. Around the large crater of Fig. 8, as previously noted, blocks of rock down to the limit of resolution (2 m) can be seen, and smaller blocks must be present outside the white line. For any given mining machine, there will be an upper limit of the size of the blocks that can be handled. For example, the mining machine designed by Sviatoslavsky and Jacobs (1988) will handle only blocks less than 40 cm in diameter. For reasons of physical minability, therefore, mining will inevitably focus on areas that have low percentages of younger craters of sufficient size and depth to penetrate bedrock. In general, the TiO_2 value assigned to a pixel will therefore be lower than the TiO_2 value of the regolith actually mined.

In summary, remote sensing of the lunar surface involving the use of spectral ratios has been extremely successful in outlining maria and parts of maria that, at surface, have TiO_2 contents ranging from 4 to more than 10%. This is a major contribution to identification of areas most favorable to the recovery of He. For Tranquillitatis it is important that three different investigations have identified the western part of the mare as a major source of high-Ti regolith. However, the northeastern area of the mare shown on the map of Johnson and others (1991) as lower in TiO_2 contents should be investigated further, because it is less disturbed by ridges, major craters, domes, and rilles and therefore could have a higher percentage of physically minable regolith than the western area.

Percentage of the Mare Physically Amenable to Mining

General Remarks

Ideally, mining areas should be flat or gently undulating. Steep-walled craters will not be minable, and the total of the areas occupied by such craters must be subtracted from the total area of the mare in calculating the total minable area. The total area of ejecta halos with coarse blocks must also be subtracted; the halos may be unminable or minable only at unacceptable costs. Ridges, rilles, and domes must be subtracted, at least until there is better knowledge of their minability. For a conservative estimate, it is probably desirable to subtract the areas occupied by rays, again until better information about these features is at hand.

In terms of information presently available, the percentage of Mare Tranquillitatis that will be physically amenable to mining cannot be fully determined, but preliminary estimates can be made from information furnished by geologic maps and photographs.

Information from Geologic Maps

The chief value of the geologic maps is the information they contain as to the extent and distribution of major features that constitute unminable ground. About 87% of the Tranquillitatis lies within the Julius Caesar and Taruntius quadrangles, so that these are the principal source of information on major features of the mare as a whole. The area of the mare occupied by major features on the two quadrangles has been calculated from measurements of the intercepts of the various features on east-west lines 1 degree apart. The results indicate that approximately 22% of the mare will be unminable owing to major structures and other major features (Table 6). If the areas occupied by rays prove to be largely or entirely minable, the figure is reduced to about 17%.

The distribution of the various features is not uniform over the mare. For an area of about 85,000 sq. km in the northeastern part of the mare (Fig. 19), the percentage covered by the features of Table 6 is only about 11.5%, of which 4% is accounted for by rays. The map of the Sabine D region gives a larger-scale view of a rectangular area 62.5 by 52 km, or 3,250 sq. km, in the southwestern part of Tranquillitatis. The Apollo 11 landing site lies within the map area, near the southwestern corner. Percentages of the total map area occupied by various major features

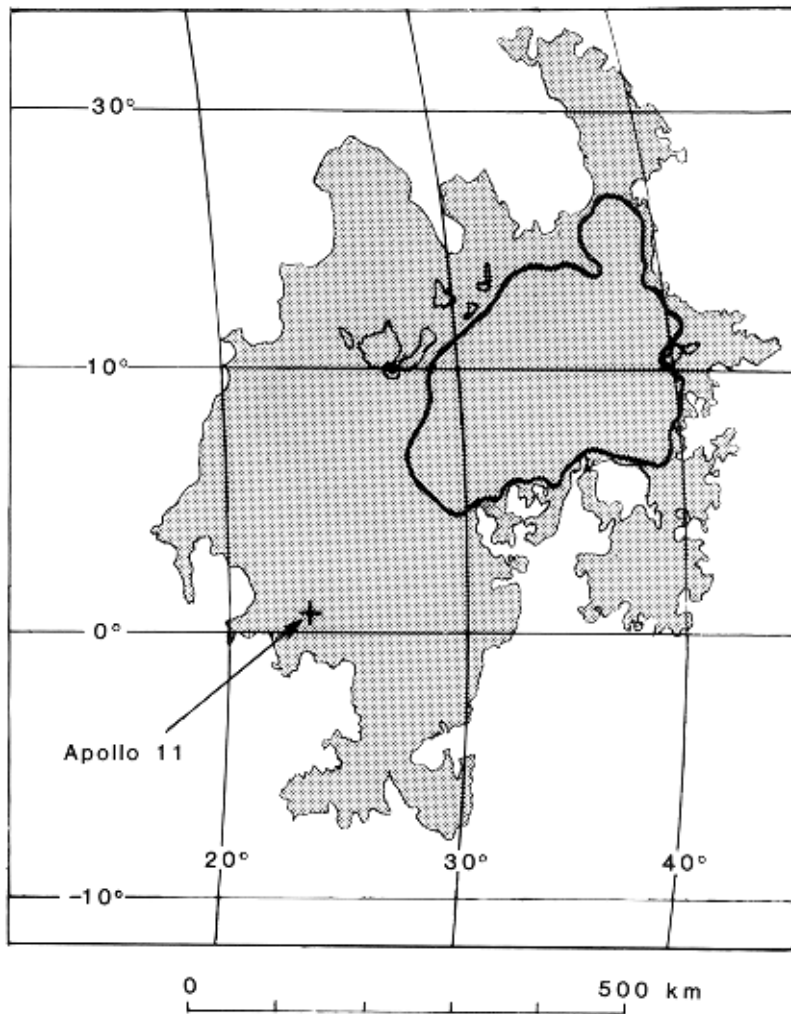


Fig. 19. Map of Mare Tranquillitatis. Major structural features are less numerous in the area bounded by the heavy black line than in the remainder of the mare.

(Table 7) have been calculated from measurements on 16 equally spaced lines 2.3 km apart and parallel to the long sides of the map. The greater number of major features in the southwestern part of Tranquillitatis and the large areas of ray material are reflected in the table. The extension of the mare southward into the Theophilus quadrangle, if mapped on the same scale as the Sabine D region, would probably show an even higher percentage of total area occupied by structural features and by ray materials mostly derived from the crater Theophilus to the south. The extension does not appear promising as a mining area and is therefore excluded from estimates of minable regolith given in this report.

Table 6

Percentages of the Total Area of Mare Tranquillitatis on the Julius Caesar and Taruntius Quadrangles Occupied by Major Features

| | |
|---------------------------------|-------|
| Domes | 0.6% |
| Ridges | 5.6 |
| Craters | 4.2 |
| Rilles | 0.6 |
| Basement rocks | 2.0 |
| Miscellaneous non-mare features | 3.4 |
| Ray materials | 5.6 |
| TOTAL | 22.0% |

Table 7

Percentages of the Sabine D Region Occupied by Major Structures and Other Features

| | |
|------------------------------|-------|
| Domes | <1.0% |
| Ridges | 4.9 |
| Craters and crater materials | 16.9 |
| Basement rocks | <1.0 |
| Ray materials | 16.0 |
| TOTAL | 38.0% |

Minable Areas as Determined from High-Resolution Photographs

Estimates of minable areas from geologic maps are only partial estimates. Their principal value is in indicating gross differences in minability between various major portions of Tranquillitatis. In order to approximate more closely the extent of minable areas, it is necessary to take into account craters and their ejecta blankets that are too small to be shown at the scales of the geologic maps.

As noted earlier, mining areas should be flat or gently undulating. Steep-walled craters will not be minable, and the total of the areas occupied by such craters must be subtracted from the total area of the mare in calculating the total minable area. The total of the areas occupied by ejecta halos with coarse blocks must also be subtracted; such halos may be unminable or minable only at unacceptable costs. Data for both craters and blocky halos must be obtained by measurements of these features on high-resolution photographs of portions of Tranquillitatis. Lunar Orbiter II high-resolution photographs were used for the present study. Photographs II-76H to II-91H make up two overlapping series that cover a rectangular area about 35 by 30 km. The Apollo 11 landing site lies 1 km outside the west boundary of this area and 4 km north of the SW corner. The Surveyor V landing site is about 14 km west of the northwest corner of the area. Except that no rilles or domes are present, the area has the full range of structural and other features displayed on Mare Tranquillitatis.

A second set of high-resolution photographs, II-67H to II-74H, covers an area 16.4 by 33 km that includes the Ranger VIII impact site. In general character this area resembles the area covered by the first set of photographs.

There are three problems in measurement of craters and ejecta halos. The first is the unbroken range of craters, from fresh craters with steep walls to very old craters that are so indistinct as to be almost unrecognizable. The fresh craters are obviously unminable. The very old craters cause only undulations of the mare surface. It seems likely (1) that such craters will pose no physical obstacles to mining and (2) will have regolith of sufficient depth and time of exposure to the solar wind to qualify as potential helium ore. However, in measuring craters, any attempt to draw a line between the two categories of craters quickly degenerates into a purely subjective exercise. I have therefore measured all craters on a given photograph, from fresh and sharp to indistinct. The result is certainly a conservative approach to estimation of unminable ground.

The second problem is that only blocks 2 m or more in diameter can be seen on the photos. Ejecta blankets outlined from the distribution of visible blocks therefore understate the extent of

blocky ground. There is no unequivocal solution of this problem. For purposes of the present study, with the advice of Harrison H. Schmitt, the following rules have been adopted:

- (1) If no blocks are visible, either in or adjacent to a crater, the unminable area is taken as a circle centered on and having the diameter of the crater.
- (2) If blocks are visible inside a crater, but not on the rim or outside it, the unminable area is taken as a circle centered on the crater and having a diameter twice that of the crater.
- (3) If blocks are visible both on the rim and outside the rim, the unminable area is taken as a circle centered on the crater and having a diameter three times that of the crater.

The validity of these rules will be established only through future experience on the Moon, but my own studies of the high-resolution photographs persuade me that the rules will yield reasonable approximations of areas potentially unminable owing to the presence of abundant blocks of bedrock and that the overall result will be a reasonable estimate of the percentage of Tranquillitatis that will be minable.

The third problem lies in errors of measurement. I estimate that for sharp-rimmed craters, the error is ± 0.2 mm for the crater diameter. As crater rims become less distinct, the accuracy of measurement undoubtedly falls off. More than this, for reasons noted above, it is not always possible to be sure what is or is not a crater, rather than an undulation of the mare surface or an artifact of the photography. Replicate measurements of a few photographs indicate that two successive sets of measurements will not agree either in the numbers of craters measured or in the total areas calculated from the measurements. The error indicated is about 10% of the percentage given; i.e., $20\% \pm 2.0\%$.

Measurements

Each high-resolution photograph covers a strip, with long dimension oriented nearly north-south, approximately 18 km long and 4.5 km wide, divided into three end-to-end prints. From south to north these are designated H₁, H₂, and H₃. Photos 83H, 84H, and 85H were initially selected for measurement as reasonably representative of the area east of the Apollo 11 landing

site. On each of the 3 prints of a photo, measurements were made for all craters with diameters 1 mm (approximately 11.7 m in actual diameter) or greater.* The results are shown in Table 8.

The series of H₂ prints from photos 84H₂ to 91H₂ give an east-west transect across the area covered by high-resolution photographs 76H to 91H. Results of measurements for the series are given in Table 9.

The tables show that there is a substantial variation in percentage of area unminable from one part of the Apollo 11 area to another. For the area of any given print, the percentage is strongly affected by the number and size of the larger craters, which are erratically distributed over the mare. However, from print to print there is variation in the density of craters; this is best indicated by the data for numbers of craters having diameters from 1 to 2 mm, but there are also variations in the density of larger craters. The effect of this on minability of portions of the mare is discussed below. Table 10 gives data for 10 high-resolution prints of the area of the Ranger VIII impact. Here again there is a considerable variation in unminable area from one print to another. Large percentages are due to large craters or areas of large craters, which are very erratically distributed over the Ranger VIII area. It is worth noting that there is no indication of this on the 1:1,000,000 map of the Julius Caesar quadrangle, and again it is clear that this map and the map of the Taruntius quadrangle have only limited value as guides to the distribution and amount of minable ground.

The successive H₂ prints, 67-H₂ to 74-H₂, give an east-west transect across the midsection of the area covered by the total assemblage of prints. It is evident from the tables that the average percentage of unminable ground is higher for the Ranger VIII area than for the Apollo 11 area, but there is marked variation in the percentage in the Ranger VIII area. In part this is due to the presence of numerous large craters. They are concentrated in one belt that runs north-south through prints 71-H₂ (northern portion), 71-H₂, and 71-H₃, and in another belt that runs

* To avoid misunderstanding, it should be pointed out that in general older craters (except the smallest ones) have younger craters superimposed on them. For example, a crater 200 m in diameter may have 30 or more superimposed visible craters. In Tables 5, 6, and 7, such a crater will be represented by a single measurement of the diameter of the large crater, from which the area occupied by the crater plus its ejecta halo, if any, will have been calculated. This area then becomes part of the total unminable area from which the percentage shown in the last column has been determined.

Table 8**Data from Photographs II-83H, II-84H, and II-85H**

| <u>Print</u> | <u>No. of Craters Measured</u> | <u>Percentage of Area Unminable</u> |
|---------------------|--------------------------------|-------------------------------------|
| II-83H ₁ | 1081 | 10.8 |
| II-83H ₂ | 575 | 22.4 |
| II-83H ₃ | 581 | 11.0 |
| II-84H ₁ | 589 | 8.9 |
| II-84H ₂ | 506 | 7.8 |
| II-84H ₃ | 736 | 8.5 |
| II-85H ₁ | 461 | 7.9 |
| II-85H ₂ | 988 | 13.0 |
| II-85H ₃ | 481 | 14.0 |
| Average | | 11.5 |

Note: In this table and in Tables 9 and 10, "Percentage of Area Unminable" means the percentage of the area of the photograph of the area occupied by craters 1 mm (11.7 m) or more in diameter plus associated halos of blocky ground. See text for explanation of rules of method of measurement.

Table 9**Data from Prints 84H₂ through 91H₂**

| <u>Print</u> | <u>No. of Craters Measured</u> | <u>Craters 1 to 2 mm in Diameter</u> | <u>Percentage of Area Unminable</u> |
|-----------------------|--------------------------------|--------------------------------------|-------------------------------------|
| II-84H ₂ | 506 | 283 | 7.8 |
| II-85H ₂ * | 639 | 560 | 14.1 |
| II-86H ₂ * | 987 | 630 | 15.4 |
| II-87H ₂ * | 775 | 507 | 11.3 |
| II-88H ₂ * | 1129 | 776 | 12.3 |
| II-89H ₂ * | 872 | 572 | 13.3 |
| II-90H ₂ * | 1331 | 887 | 13.1 |
| II-91H ₂ * | 902 | 622 | 12.8 |
| Average | | | 12.5 |

*Overlap with previous print excluded from measurement; e.g., the portion of 85H₂ overlapping 84H₂ is excluded, and so on.

Table 10

Data from Photographs II-67H to II-74H

| <u>Print</u> | <u>No. of Craters Measured</u> | <u>Percentage of Area Unminable</u> |
|---------------------|--------------------------------|-------------------------------------|
| II-67H ₁ | 796 | 10.9 |
| II-67H ₂ | 664 | 23.2 |
| II-67H ₃ | 549 | 25.9 |
| II-68H ₂ | 806 | 15.0 |
| II-69H ₂ | 847 | 12.1 |
| II-70H ₁ | 597 | 26.1 |
| II-70H ₂ | 930 | 11.1 |
| II-71H ₂ | 520 | 50.4 |
| II-72H ₁ | 780 | 20.1 |
| II-72H ₂ | 740 | 16.4 |
| II-73H ₂ | 619 | 39.0 |
| II-74H ₂ | 883 | 15.8 |
| Average | | 22.2 |

northwest-southeast through 72-H₃, 73-H₃, and 73-H₂. Print 71-H₂ (Fig. 20) is representative of the first belt. It has not only large craters but closely spaced craters of intermediate size. As indicated in Table 10, half the area of the print must be considered unminable, with adjacent portions of 71-H₁ and 71-H₃. Northern 72-H₂ and the southern part of 72-H₃ are similar. On the total assemblage of prints, however, there are large areas for which the unminable percentage will range from about 12 to 15%.

Other Factors Affecting Minability

The minability of a portion of a mare is affected by other factors besides crater-halo area; namely, crater distribution over the area, crater size distribution, and the capability of the mining system for excavating blocky material along with the finer regolith and rejecting all coarse material so as to process only the fines. The first factor is illustrated in Fig. 22. This chart is an overlay of print II-84H₃ (Fig. 21). Each circle on the chart represents a crater, with its halo of ejecta if present, the extent of the halo being determined according to the rules for measurement described

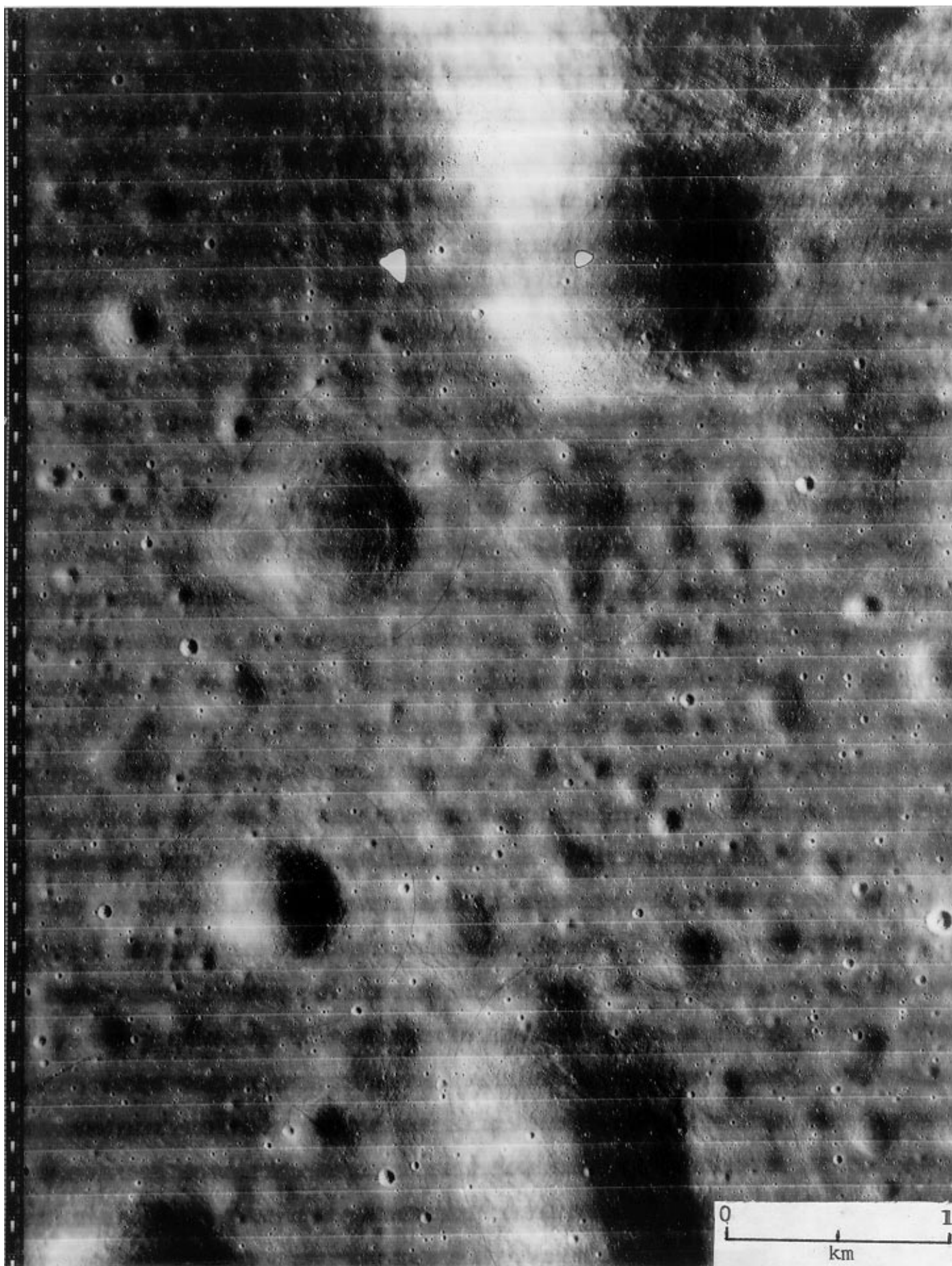


Fig. 20. Lunar Orbiter photograph 71H₂, reduced from original size of 40 × 90 cm.

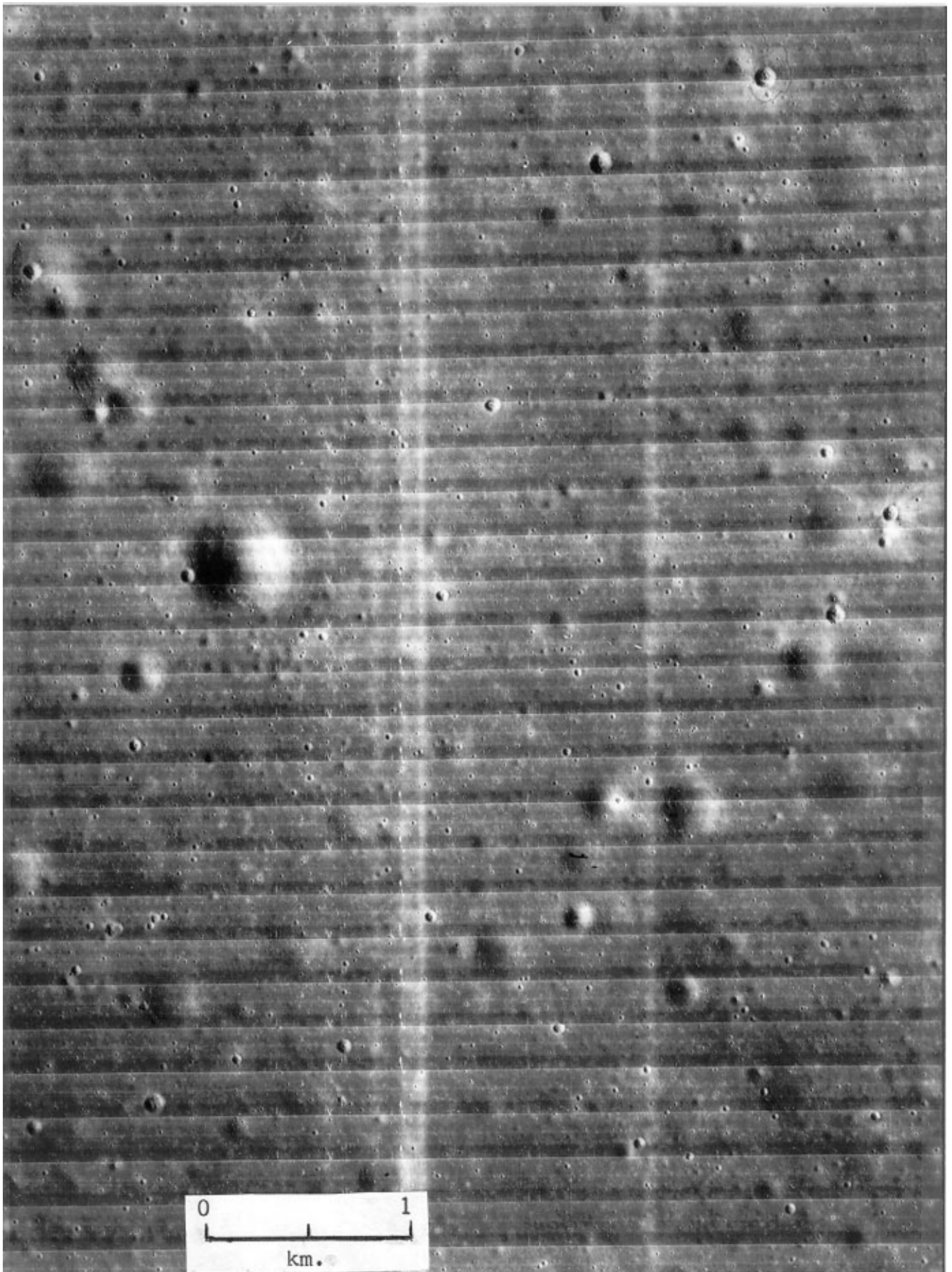


Fig. 21. Lunar Orbiter photograph II-84H₃, reduced from original size of 40 × 90 cm. The scale is 1 km in length. Note the range in distinctness of the craters.

above. The center of each circle is the center of the crater. The minimum thickness of regolith is assumed as 3 m outside craters and halos. The chart clearly indicates the effect of distribution on the size of intervening minable areas. The worst possible case is one in which the craters are evenly distributed. This will produce minable areas of minimum size. The best case is that of pronounced clustering of craters; minable area will then be much larger.

The effect of size distribution is best considered in conjunction with the capability of the mining system for handling blocky material. The effect of the latter is clearly shown by a comparison of Figs. 22 and 23. In Fig. 22 it is assumed that the mining system cannot handle blocky material. It must therefore avoid all craters 1 mm (11.7 m) or more in diameter on the photographs since these may be accompanied by blocky halos. Suppose that the minimum area for an efficient mining unit is 400 m by 400 m. The figure shows that the number of mining areas available is very limited. If, however, the mining system is capable of sorting out blocks from the regolith and discarding them, craters up to 2.0 mm (23.4 m) in diameter on the photographs can be mined. The number and size of mining areas available is greatly increased. For the case illustrated in Fig. 22, the percentage of the total area minable would not exceed 15%. In the case of Fig. 23 the minable area of 400 m square blocks plus contiguous extensions would exceed 40%. The significance of the size distribution of craters now becomes apparent. The total number of craters in an area may be large, but if there is a significant fraction in the 1.0 to 2.0 mm (11.7 to 23.4 m) range, a substantial percentage of the total area may still be minable.

Assuming an average minable regolith thickness of 3 m and a regolith density of 2.0, the total minable regolith in unit blocks and sideward extensions in the area of Fig. 23 is 71,400,000 tonnes. At the mining rate of 4,960,000 tonnes per year estimated for the machine designed by Sviatoslavsky and Jacobs (1988), the area would supply the machine for 14.4 years.

Pending analysis of the cost effectiveness of mining in relation to the design of mining machines and the size of mining units required for efficient operation, the selection of a 400-meter square mining unit is arbitrary. If it proves economically feasible to mine smaller units, the minable percentage of the total area will be increased. In Fig. 24 the basic mining unit is taken as

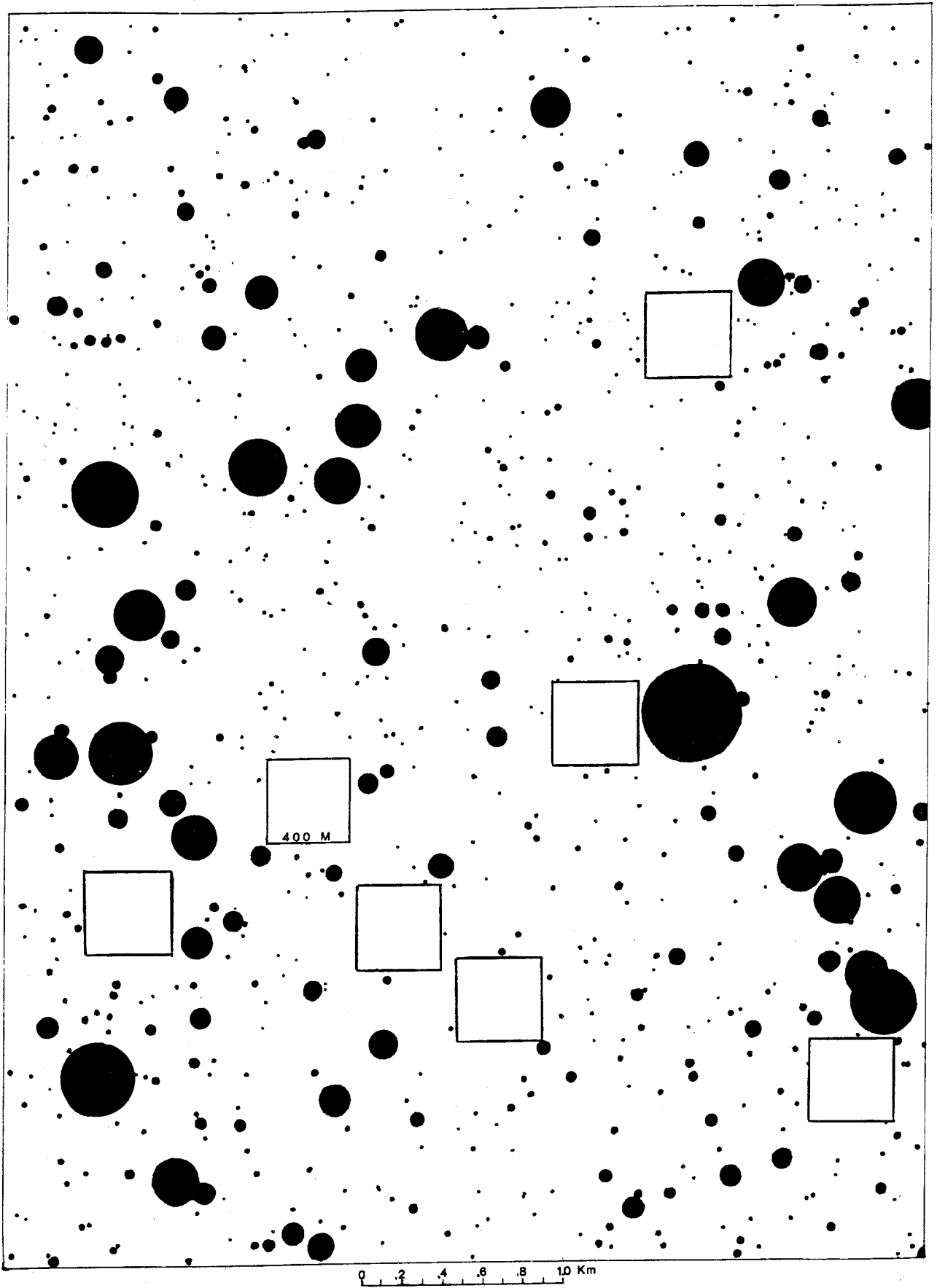


Fig. 22. Craters 11.7 m or more in diameter, with their inferred ejecta halos, plotted on an overlay of Fig. 21. Unit mining blocks are 400 m square.

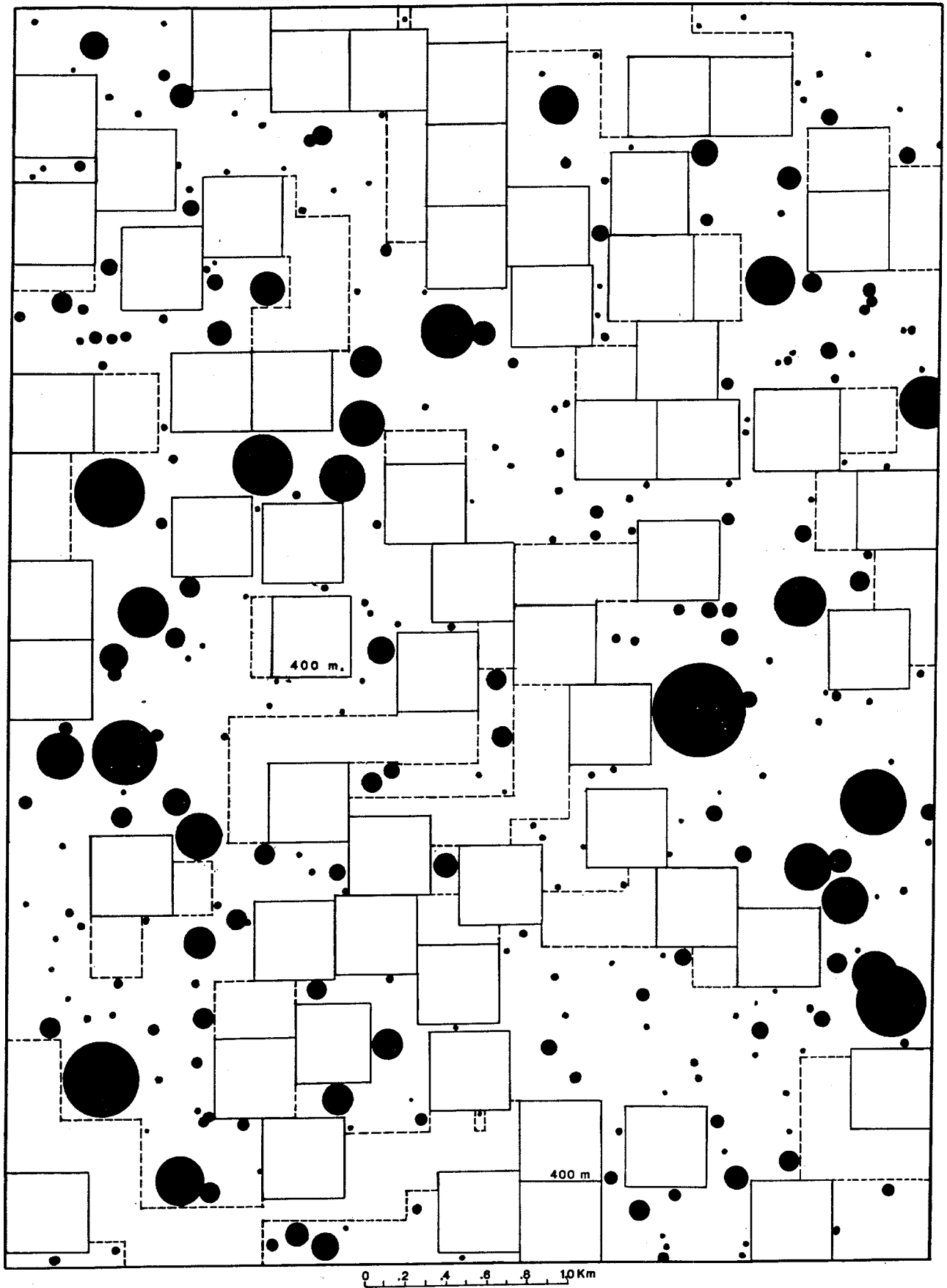


Fig. 23. Craters 11.7 m or more in diameter, with their inferred ejecta halos, plotted on an overlay of Fig. 21. Unit mining blocks are 400 m square; possible extensions are shown by dashed lines.

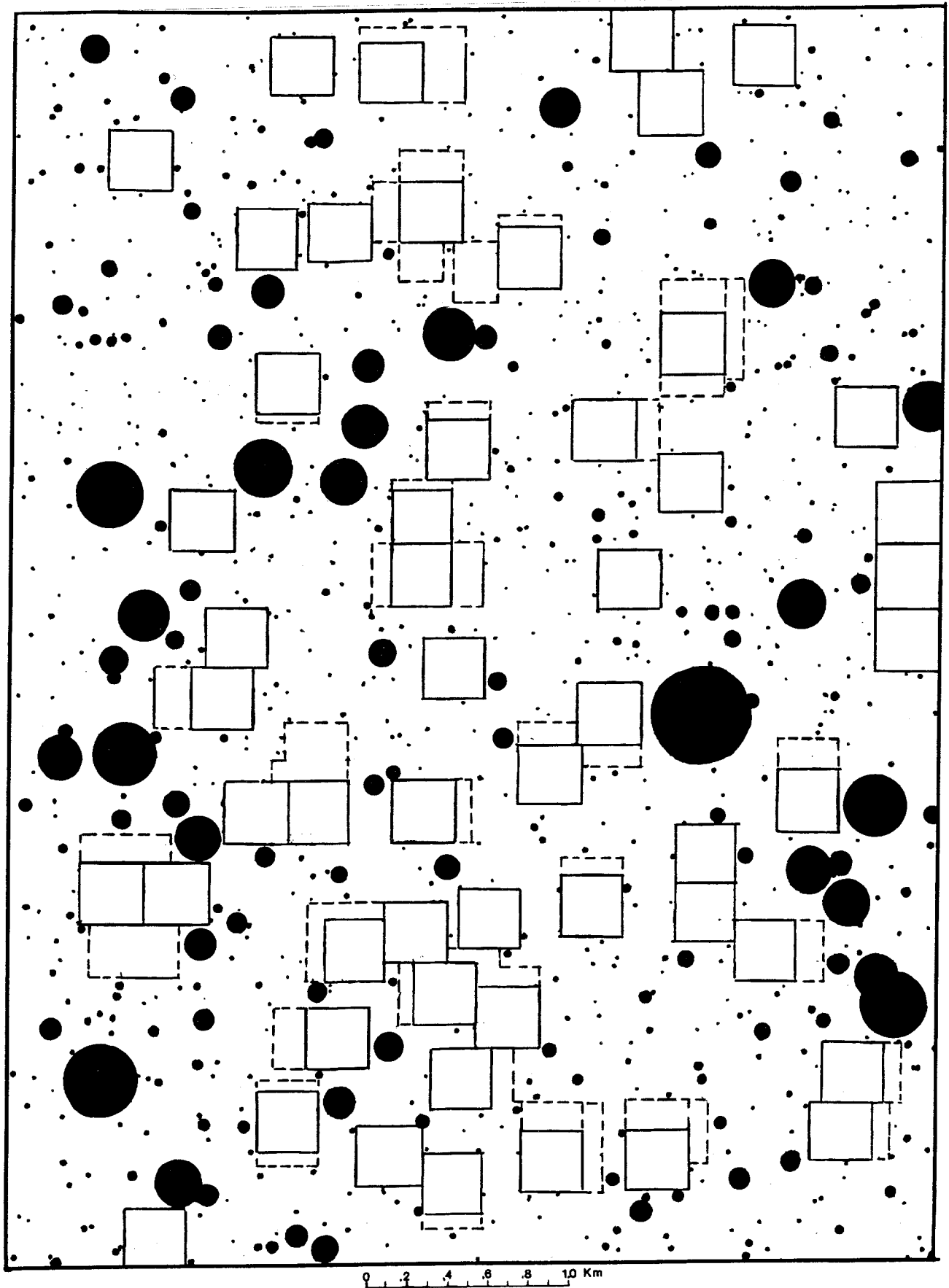


Fig. 24. Craters 11.7 m or more in diameter, with their inferred ejecta halos, plotted on an overlay of Fig. 21. Unit blocks are 300 m square; possible extensions are shown by dashed lines.

300 meters square, but no blocks can be handled, hence craters 11.7 m or more in diameter must be avoided. The minable percentage of the area is about 22%. In Fig. 25, craters less than 23.4 m in diameter can be mined. The minable percentage in unit blocks and sideward extensions is 56%, and the amount of regolith available is 95,200,000 tonnes.

Charts similar to those of Fig. 22 through 25 have been plotted for three additional prints for which the calculated percentages unminable due to craters and halos are 12.1 (II-88H₂), 15.2 (II-86H₂), and 22.1% (II-83H₂). The effect of unit block size on percentage of total area minable is shown in Fig. 26. For the area covered by each print, minable percentage reaches its maximum when the unit block size becomes zero, at which point the unminable area is equal to the percentage of the total area occupied by craters and blocky ejecta halos. It is evident that for any given area, the design of the mining equipment, in particular its maneuverability, will strongly affect the minable percentage.

The study suggests that for the Apollo 11 area minable portions will range from about 17% to 42% if the basic mining unit is 400 m square and the mining system can handle small blocks, or from 28 to 57% if the basic mining unit is 300 m square. If the system is capable of mining smaller blocks and irregular extensions of blocks, these percentages will be increased.

Amount of Helium in Movable Regolith of Mare Tranquillitatis

In my previous report (Cameron, 1990) the data developed in preparing Fig. 15 were used as the basis for an estimate of tonnage and grade of the regolith of Mare Tranquillitatis and an estimate of the amounts of He and He-3 available in it. The area of the mare was estimated at roughly 300,000 sq. km, of which it was estimated that as much as 50% may be minable with a suitable mining system. The average thickness of regolith was taken as 3 m, although a greater average thickness appears to be indicated. Of the total area of the mare it was inferred that 28% is covered by regolith (category A) that contains 30 to 45 wppm total He, 65% by regolith (category B) that contains 20 to 30 wppm total He, and 7% by regolith (category C) that contains less than 20 wppm total He. The third category is too low in He to be of interest at present. Areas

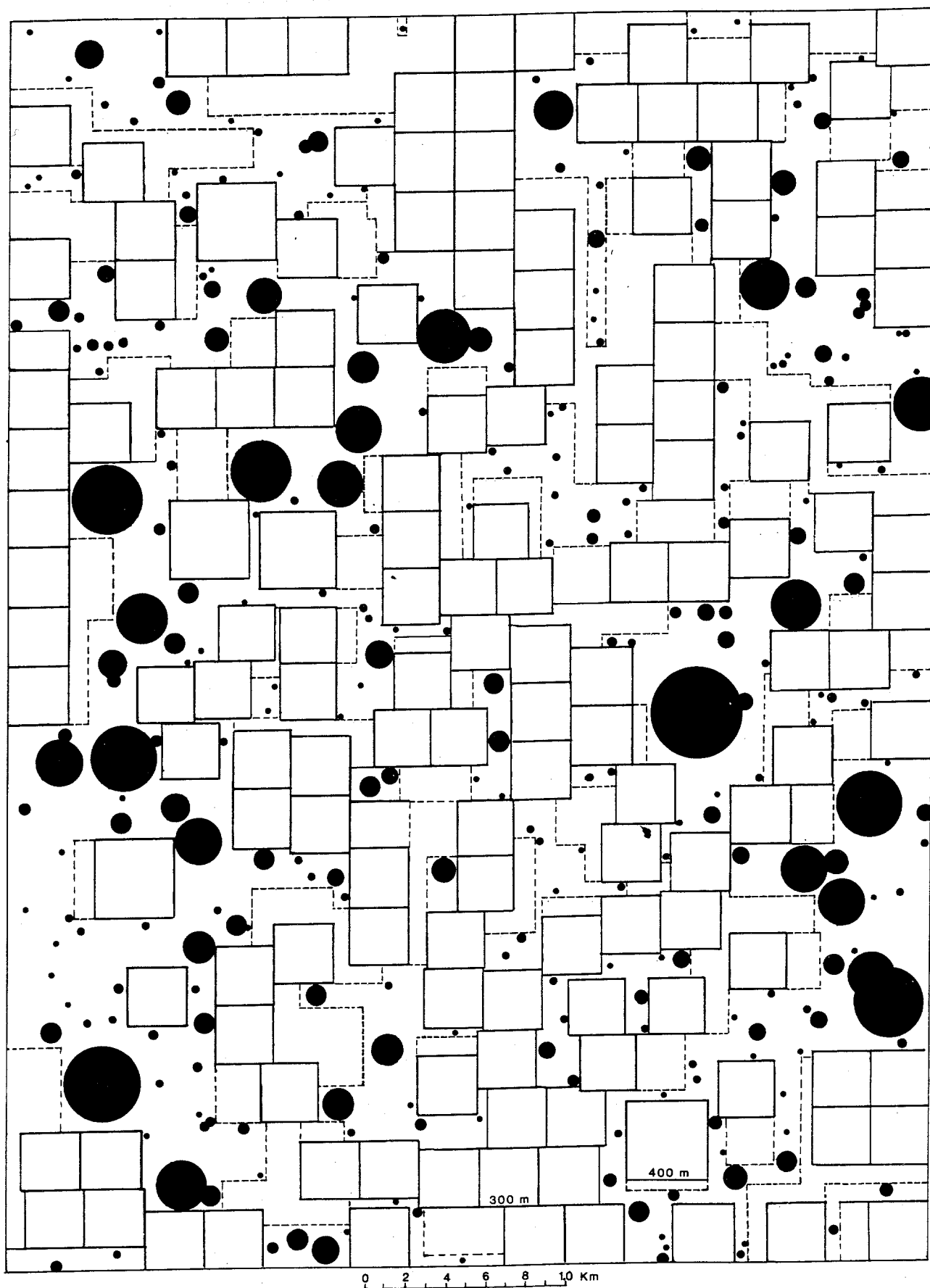


Fig. 25. Craters 23.4 m or more in diameter, with their inferred ejecta halos, plotted on an overlay of Fig. 21. Unit blocks are 300 m square; possible extensions are shown by dashed lines.

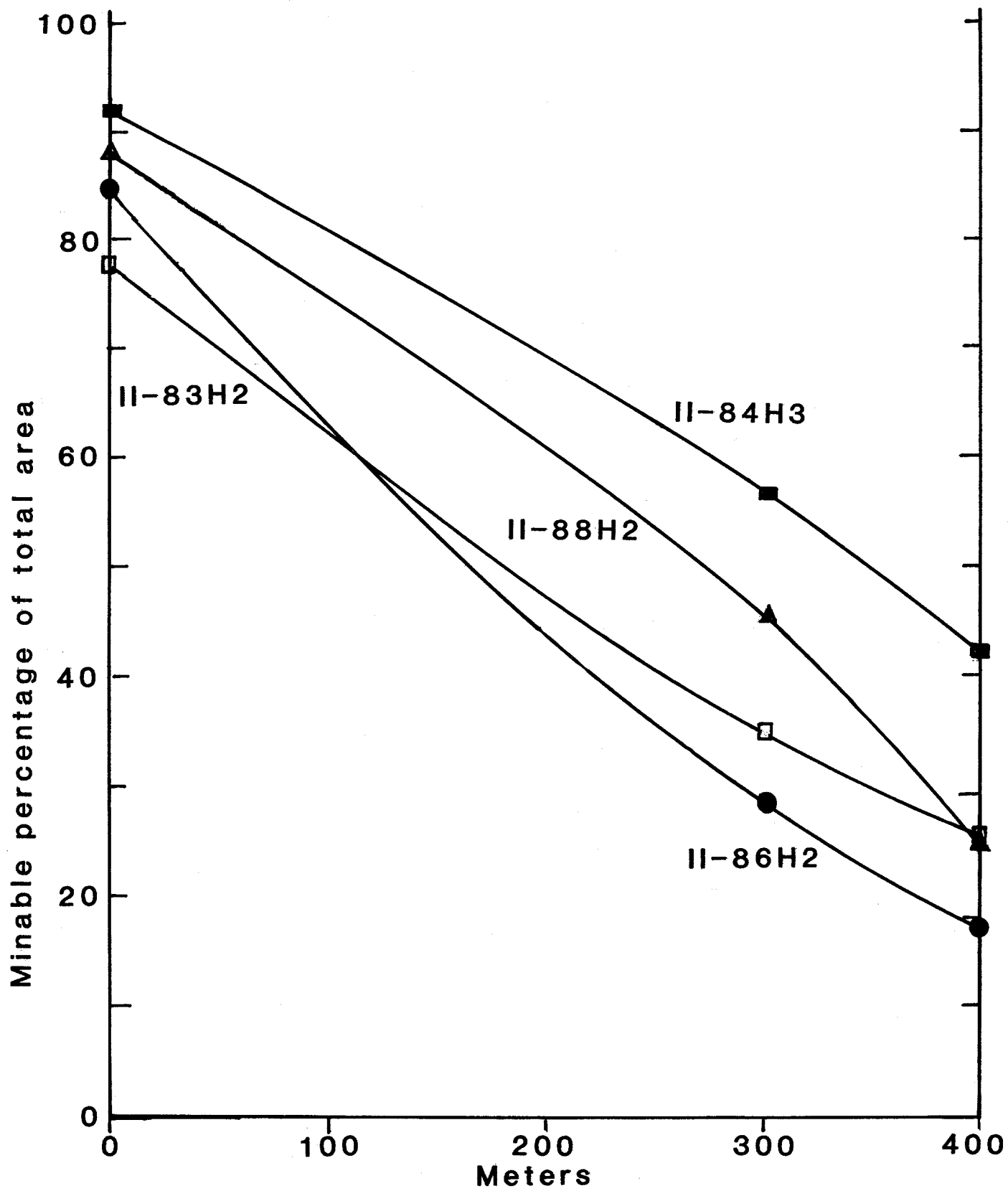


Fig.26. Mirable percentage of total area in relation to size of unit mining block.

Table 11

Minable Regolith and Helium Content of Mare Tranquillitatis

| <u>Regolith Category</u> | <u>Area in km²</u> | <u>Average He Content wppm</u> | <u>Regolith Minable tonnes</u> | <u>He tonnes</u> | <u>³He tonnes</u> |
|--------------------------|-------------------------------|--------------------------------|--------------------------------|-------------------------|------------------------------|
| A | 84,000 | 38 | 252 x 10 ⁹ | 9.58 x 10 ⁶ | 2,726 |
| B | 195,000 | 25 | 598 x 10 ⁹ | 14.96 x 10 ⁶ | 4,315 |
| Totals | 279,000 | | 850 x 10 ⁹ | 24.54 x 10 ⁶ | 7,041 |

and minable tonnages of regolith, He, and He-3 represented in the first two categories are given in Table 11. Assumptions are: (1) 50% minability, (2) regolith thickness 3 m, and He (total)/He-3 = 2600.

The estimates of minable areas in categories A and B may not allow sufficiently for areas unminable owing to major features, since these may not be adequately represented on the high-resolution photographs of the Apollo 11 and Ranger VIII areas. In my judgment, however, any resulting overestimate is likely to be more than offset by underestimate of minable areas due to classification of all indistinct craters as unminable, and to use of an average regolith depth of 3 m.

The estimate of Table 11 is a preliminary estimate. It will need revision on the basis of systematic sampling of the regolith of Mare Tranquillitatis and resolution of discrepancies in present reflectance data. Meanwhile the estimate serves to indicate that the mare is a potential major source of He-3; 25 tonnes of He-3 contains sufficient energy to supply U.S. requirements of electrical energy for one year at the 1991 rate of use.

OTHER AREAS OF HIGH-TITANIUM REGOLITH

Remote sensing indicates that other areas of high-Ti regolith occur on the nearside of the Moon. Figure 27 shows the distribution of color groups of basaltic regolith indicated by spectral reflectance studies, with the inferred TiO₂ contents of each group. Substantial areas of high-TiO₂ regolith are indicated in Oceanus Procellarum, Mare Imbrium, Mare Humorum, and Mare Nubium,

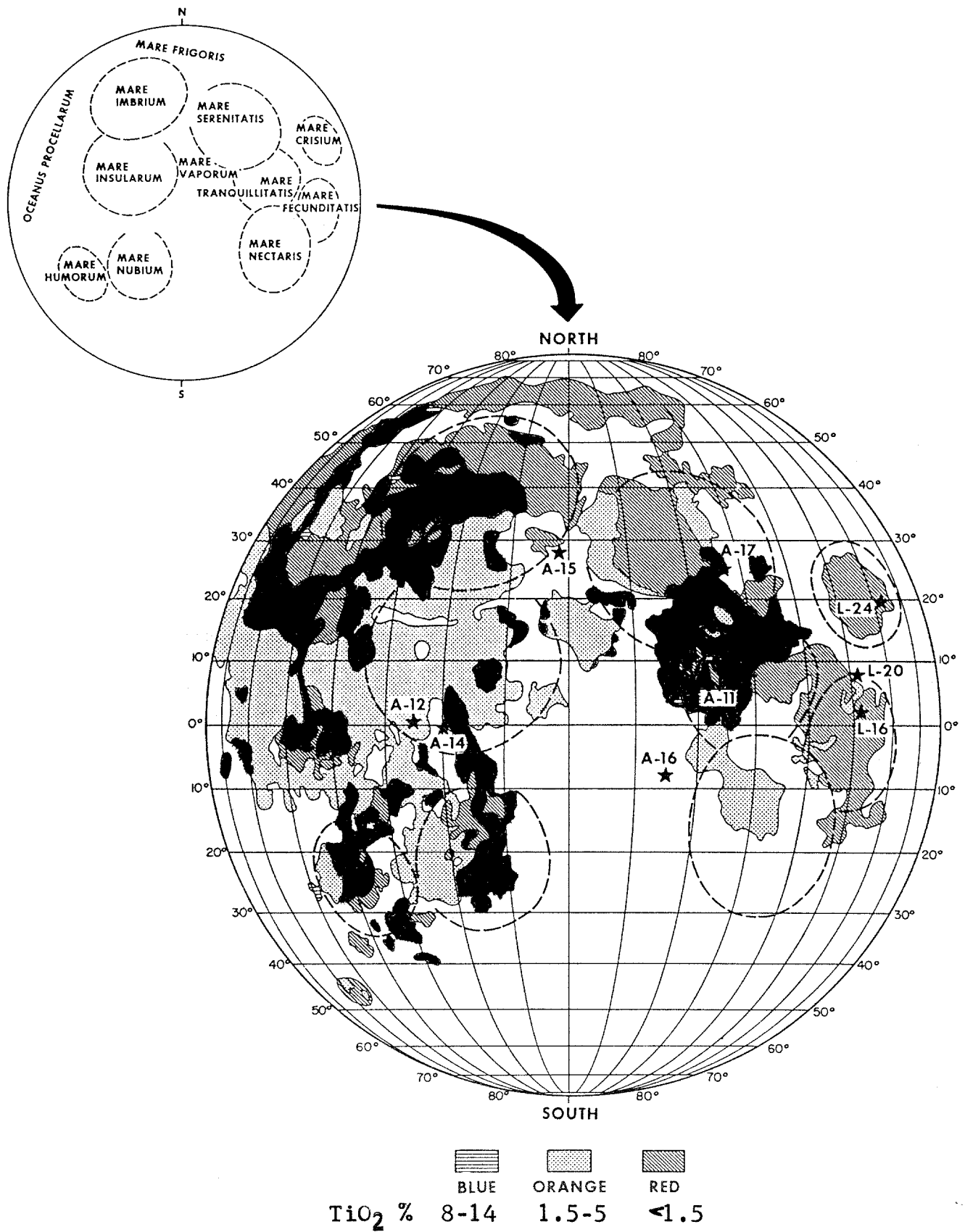


Fig. 27. Color groups of mare regoliths and the TiO₂ values thought to be represented by the groups. From Basaltic Volcanism Study Project, 1981, Lunar mare basalts. In Basaltic Volcanism on the Terrestrial Planets, Pergamon Press, pp. 236-267.

and smaller areas occur in Mare Insularum and southwest of Mare Serenitatis. No samples of regolith of those areas are yet available, and their spectral characteristics apparently are not identical with those of Mare Tranquillitatis and the Taurus-Littrow area, where Apollo 17 sampled high-TiO₂ regolith that appears to be an extension of the regolith of Tranquillitatis along the southeast side of Mare Serenitatis. The TiO₂ abundance map of the lunar nearside by Johnson and others (1991) does not agree with Fig. 27; the western areas are shown as occupied by regolith containing 5 to 6% TiO₂, with a few areas on Procellarum containing 7% TiO₂. The new spectral ratio map resulting from scanning by Galileo (Belton and others, 1992) appears to indicate high-TiO₂ regolith on most of the areas indicated as such on Fig. 26, but the spectral units shown on the map have not yet been quantified. Further investigation of the areas, supported by sampling, will be necessary to indicate the potential of the areas.

SUMMARY AND CONCLUSIONS

- 1) Mare Tranquillitatis occupies an area of about 300,000 sq. km on the near side of the Moon.
- 2) Major structural features, probably all unminable, are ridges, rilles, domes, islands of basement rocks, and major craters. They are most numerous in the western half of the mare. Ray materials are also present in parts of the mare, mostly in the western part. Their effect on minability is uncertain.
- 3) Regolith of Mare Tranquillitatis is derived predominantly from underlying basaltic volcanics but is diluted, to varying degrees, by ejecta composed of highland material.
- 4) Studies of small craters indicate an average thickness of regolith, away from larger craters, in excess of 3 m.
- 5) The regolith consists predominantly of fine-grained (less than 100 μm) particles. Helium is concentrated in the fine-grained material.
- 6) From part to part of the mare the average helium content of regolith, as inferred from sampling by Apollo 11 and from remote sensing, ranges from less than 20 wppm to at least 45 wppm. Both lateral and vertical small-scale variations are to be expected.

- 7) Decline in average He content of regolith with depth is not indicated by available data over a range of at least several meters and, given the nature of the impact gardening process, is not to be expected.
- 8) In the earlier version of this report, it was estimated from remote sensing and sampling data then available that 28% of the mare is occupied by regolith with 30-45 wppm He, about 65% by regolith with 20-30% wppm, and 7% by regolith with less than 20 wppm. However, further sampling and calibration of reflectance data are needed to resolve discrepancies in present data.
- 9) The percentage of a given area of the mare that is physically amenable to mining is determined fundamentally by the number, size and size distribution of medium-sized to small craters. However, the percentage will be strongly affected by the nature of the mining system, especially by its ability to handle ejecta blocks and by its maneuverability.
- 10) Assuming a capability for handling small ejecta blocks, and cost-efficient mining of unit blocks as small as 300 m square, measurements of craters and associated ejecta halos on high-resolution photographs indicate that from place to place the percentage of the mare physically minable will range from 28 to 57%. Minability of an average 40% seems assured. With design of mining machinery so as to permit mining of somewhat smaller unit areas, 50% minability should be achievable.
- 11) Assuming that the regolith averages 3 m in thickness and that 50% will be minable, I have estimated that Mare Tranquillitatis contains 2,726 tonnes of He-3 in minable regolith containing 30-45 wppm total He, and 4,315 tonnes of He-3 in regolith with 20-30 wppm total He. This is a preliminary estimate, but it indicates that Tranquillitatis is a potential major source of He-3.
- 12) The western part of Mare Tranquillitatis, in which Ranger VIII and Apollo 11 landed, presents numerous obstacles to helium mining. Particularly in the southern part of this area, there are numerous prominent ridges and large patches of ray materials. In a belt near the

western margin of the mare, there is a series of large craters, up to 45 km in diameter, and a group of volcanic domes up to about 20 km in diameter.

- 13) The 85,000 sq. km area of the northeastern part of the mare is much freer of major craters and ridges and appears much more amenable to mining than the western part of the mare. However, the TiO_2 content of its regolith, hence its He content, is presently in doubt.
- 14) Verification of the helium potential of Mare Tranquillitatis should be a principal objective of future lunar missions.

ACKNOWLEDGMENTS

I am greatly indebted to Paul D. Spudis for providing geologic maps and for furnishing other information that has assisted this study. I am also indebted to Harrison H. Schmitt for numerous suggestions and for a critical review of the original version of this report.

REFERENCES

- Basaltic Volcanism Study Project, 1981, Lunar mare basalts. In *Basaltic Volcanism on the Terrestrial Planets*, Pergamon Press, pp. 236-267.
- Beaty, D.W., and A.L. Albee, 1978, Comparative petrology and possible genetic relations among the Apollo 11 basalts. *Proc. 9th Lunar Planet. Sci. Conf.*, vol. 1, pp. 359-463.
- Beaty, D.W., and A.L. Albee, 1980, The geology and petrology of the Apollo 11 landing site. *Proc. 11th Lunar Planet. Sci. Conf.*, vol. 1, pp. 23-35.
- Belton, M.J.S., J.W. Head III, C.M. Pieters, R. Greeley, A.S. McEwen, G. Neukom, K.P. Klaasen, C.D. Anger, M.H. Carr, C.R. Chapman, M.E. Davies, F.P. Fanale, P.J. Gierasch, R. Greenberg, A.P. Ingersoll, T. Johnson, B. Paczkowski, C.B. Pilcher, and J. Veverka, 1992, Lunar impact basins and crustal heterogeneity: new western limb and farside data from Galileo. *Science*, vol. 255, pp. 570-576.
- Bogard, D.D., and W.C. Hirsch, 1978, Noble gases in Luna 24 core. In *Mare Crisium: The View from Luna 24*. Pergamon Press, New York, pp. 105-116.
- Bogard, D.D., and L.E. Nyquist, 1972, Noble gas studies on regolith materials from Apollo 14 and 15. *Proc. 3rd Lunar Sci. Conf.*, vol. 2, pp. 1797-1820.
- Cameron, E.N., 1970, Opaque minerals in certain lunar rocks from Apollo 11. *Proc. Apollo 11 Lunar Sci. Conf.*, vol. 1, pp. 221-245.
- Cameron, E.N., 1987, Titanium in lunar regoliths and its use in selecting He-3 mining sites. Wisconsin Center for Space Automation and Robotics, Report No. WCSAR-TR-AR3-8708.
- Cameron, E.N., 1988, Mining for helium - site selection and evaluation. *Proc. 2nd Symposium on Lunar Bases and Space Activities of the 21st Century*, Houston, TX, in press.
- Cameron, E.N., 1990, Geology of Mare Tranquillitatis and its significance for the mining of helium. Wisconsin Center for Space Automation and Robotics, Report No. WCSAR-TR-AR3-9001-1, 62 pp.

- Cameron, E.N., and G.L. Kulcinski, 1992, Helium-3 from the Moon - An alternative source of energy. Proc. 1st International Conference on Environmental Issues and Waste Management in Energy and Mineral Production, T.M. Yegulalp and K. Kim, eds., Battelle Memorial Press, pp. 319-357.
- Carr, M.H., 1965, Geologic map of the Mare Serenitatis quadrangle of the Moon. USGS Map I-4899 (LAC-42).
- Criswell, D.R., and R.D. Waldron, 1982, Lunar utilization. In *Space Utilization*, B. O'Leary, ed., vol. II, CRC Press, Boca Raton, FL, pp. 1-53.
- Cuttitta, F., H.J. Rose, Jr., C.S. Ansell, M.K. Carron, R.P. Christian, E.J. Dwornik, L.P. Greenland, A.W. Helz, and D.T. Ligon, Jr., 1971, Elemental composition of some Apollo 12 lunar rocks and soils. Proc. 2nd Lunar Sci. Conf., vol. 2, pp. 1217-1229.
- Cuttitta, F., H.J. Rose, Jr., C.S. Ansell, M.K. Carron, R.P. Christian, D.T. Ligon, Jr., E.J. Dwornik, T.L. Wright, and L.P. Greenland, 1973, Chemistry of twenty-one igneous rocks and soils returned by the Apollo 15 mission. Proc. 4th Lunar Sci. Conf., vol. 2, pp. 1081-1096.
- Eberhardt, P., J. Geiss, H. Graf, N. Grögler, U. Krähenbühl, H. Schwaller, J. Schwarzmüller, and A. Stettler, 1970, Trapped solar wind noble gases, exposure age and K/Ar age in Apollo 11 lunar fine material. Proc. Apollo 11 Lunar Sci. Conf., pp. 1037-1070.
- Eberhardt, P., J. Geiss, H. Graf, N. Grögler, M.D. Mendia, M. Mörgeli, H. Schwaller, and A. Stettler, 1972, Trapped solar wind noble gases in Apollo 12 lunar fines 12002 and Apollo 11 breccia 10046. Proc. 3rd Lunar Sci. Conf., pp. 1821-1856.
- Elston, D.P., 1972, Geologic map of the Colombo quadrangle of the Moon. USGS Map I-714 (LAC-79).
- Eugster, O., P. Eberhardt, J. Geiss, N. Grögler, M. Jungck, and M. Mörgeli, 1975, Solar-wind-trapped and cosmic-ray-produced noble gases in Luna 20 soil. Proc. 6th Lunar Sci. Conf., pp. 1989-2007.

- Funkhouser, J., E. Jessberger, O. Muller, and J. Zahringer, 1970, Active and inert gases in Apollo 12 and Apollo 11 samples released by crushing at room temperature and by heating at low temperatures. Proc. 2nd Lunar Sci. Conf., vol. 2, pp. 1381-1396.
- Grolier, M.J., 1970, Geologic map of the Sabine D region of the Moon, USGS Map I-618 [ORB II-6 (100)].
- Grolier, M.J., 1970, Geologic map of the Apollo 11 Landing Site 2. USGS Map I-619 [ORB II-6 (25)].
- Haskin, L.A., P.A. Helmke, D.F. Blanchard, J.W. Jacobs, and K. Telander, 1973, Major and trace element abundances in samples from the lunar highlands. Proc. 4th Lunar Sci. Conf., vol. 2, pp. 1275-1296.
- Heymann, D., J.L. Jordan, A. Walker, M. Dziczkaniec, J. Ray, and R. Palma, 1978, Inert gas measurements in the Apollo 16 drill core and an evaluation of the stratigraphy and depositional history of this core. Proc. 9th Lunar Sci. Conf., vol. 2, pp. 1885-1912.
- Heymann, D., S. Lakatos, and J.R. Walton, 1973, Inert gases in a terra sample. *Geochimica Geocosmica Acta*, vol. 37, pp. 875-885.
- Heymann, D., and A. Yaniv, 1970, Inert gases in the fines from the Sea of Tranquillity. Proc. Apollo 11 Lunar Sci. Conf., vol. 2, pp. 1247-1259.
- Heymann, D., A. Yaniv, and S. Lakatos, 1972a, Inert gases in 12 particles and one dust sample from Luna 16. *Earth Planet. Sci. Letters*, vol. 13, pp. 400-406.
- Heymann, D., A. Yaniv, and S. Lakatos, 1972b, Inert gases from Apollo 12, 14, and 15 fines. Proc. 3rd Lunar Sci. Conf., vol. 2, pp. 1857-1863.
- Hintenberger, H., H.W. Weber, H. Voshage, H. Wänke, F. Begemann, and F. Wlotzka, 1970, Concentrations and isotopic abundances of the rare gases, hydrogen, and nitrogen in lunar matter. Proc. Apollo 11 Lunar Sci. Conf., vol. 2, pp. 1269-1282.
- Hintenberger, H., H.W. Weber, and N. Takaokoka, 1971, Concentration and isotopic abundances of rare gases in lunar matter. Proc. 2nd Lunar Sci. Conf., vol. 2, pp. 1617-1626.

- Hintenberger, H., and H.W. Weber, 1973, Trapped rare gases in lunar fines and breccias. Proc. 4th Lunar Sci. Conf., pp. 2003-2020.
- Hintenberger, H., H.W. Weber, and L. Schultz, 1974, Solar, spallogenic, and radiogenic rare gases on Apollo 17 soils and breccias. Proc. 5th Lunar Sci. Conf., vol. 2, pp. 2005-2022.
- Hintenberger, H., L. Schultz, and H.W. Weber, 1975, A comparison of noble gases in lunar fines and soil breccias. Proc. 6th Lunar Sci. Conf., vol. 2, pp. 2261-2270.
- Hübner, W., D. Heymann, and T. Kirsten, 1973, Inert gas stratigraphy of Apollo 15 core sections 15001 and 15003. Proc. 4th Lunar Sci. Conf., vol. 2, pp. 2021-2036.
- Hübner, W., T. Kirsten, and J. Kiko, 1975, Rare gases in Apollo 17 soils with emphasis on analysis of size and mineral fractions of soil 74241. Proc. 6th Lunar Sci. Conf., vol. 2, pp. 2009-2026.
- Johnson, T.V., R.S. Saunders, D.L. Matson, and J.L. Mosher, 1977, A TiO₂ abundance map for the northern maria. Proc. 8th Lunar Sci. Conf., vol. 1, pp. 1029-1036.
- Jordan, J.L., 1989, Prediction of He distribution at the lunar surface. Proc. Symposium on Space Mining and Manufacturing, Univ. of Arizona, Tucson, AZ, pp. VII-38 to VII-51.
- Kirsten, O. Muller, F. Steinbrunn, and J. Zähringer, 1970, Study of distribution and variations of rare gases in lunar material by a microprobe technique. Proc. Apollo 11 Lunar Sci. Conf., vol. 2, pp. 1331-1343.
- Kirsten, T., F. Steinbrunn, and J. Zähringer, 1971, Location and variation of trapped rare gases in Apollo 12 lunar samples. Proc. 2nd Lunar Sci. Conf., vol. 2, pp. 1651-1669.
- Kirsten, T., J. Deubner, P. Horn, I. Kaneoka, J. Kiko, O.A. Schaeffer, and S.K. Thio, 1972, The rare gas record of Apollo 14 and 15 samples. Proc. 3rd Lunar Sci. Conf., vol. 2, pp. 1865-1890.
- Laul, J.C., D.W. Hill, and R.A. Schmitt, 1974, Chemical studies of Apollo 16 and 17 samples. Proc. 5th Lunar Sci. Conf., vol. 2, pp. 1047-1066.
- Laul, J.C., and R.A. Schmitt, 1973, Chemical composition of Apollo 15, 16, and 17 samples. Proc. 4th Lunar Sci. Conf., vol. 2, pp. 1349-1367.

- Laul, J.C., and J.J. Papike, 1980a, The lunar regolith: comparative chemistry of the Apollo sites. Proc. 12th Lunar Planet. Sci. Conf., vol. 2, pp. 1307-1340.
- Laul, J.C., and J.J. Papike, 1980b, The Apollo 17 drill core: Chemistry of size fractions and the nature of the fused soil component. Proc. 11th Lunar Planet. Sci. Conf., vol. 2, pp. 1395-1413.
- Ma, M.S., R.A. Schmitt, G.J. Taylor, R.D. Warner, D.E. Langer, and K. Keil, 1978, Chemistry and petrology of Luna 24 lithic fragments and -250 μm soils: Constraints on the origin of VLT basalts. In *Mare Crisium: The View from Luna 24*, Pergamon Press, New York, pp. 569-592.
- Marti, K., G.W. Lugmair, and H.C. Urey, 1970, Solar wind gases, cosmic-ray spallation products and the irradiation history of Apollo 11 samples. Proc. Apollo 11 Lunar Sci. Conf., vol. 2, pp. 1357-1367.
- Melandrez, D.J., 1992, High spatial resolution mapping of lunar mare titanium abundances. SERC Newsletter, Univ. of Arizona, pp. 12-13.
- Melosh, H.J., 1989, Cratering, A Geologic Process. Oxford University Press, New York, 245 pp.
- Milton, D.J., 1968, Geologic map of the Theophilus quadrangle. USGS Map I-546 (LAC-78).
- Moore, H.J., J.M. Boyce, G.G. Schaber, and D.H. Scott, 1980, Lunar remote sensing and measurements. U.S. Geol. Survey, Prof. Paper 1046-B, pp. B71-B78.
- Morris, E.C., and D.E. Wilhelms, 1967, Geologic map of the Julius Caesar quadrangle of the Moon. USGS Map I-510 (LAC-60).
- Nava, D.F., 1974, Chemical compositions of some soils and rocks from the Apollo 15, 16, and 17 lunar sites. Proc. 5th Lunar Sci. Conf., vol. 2, pp. 1087-1096.
- Nakamura, Y., J. Dorman, F. Duennebier, D. Laemmlein, and G. Latham, Shallow lunar structure determined from the passive seismic experiment. *Moon*, 13, pp. 57-66.
- Papike, J.J., S.B. Simon, and J.C. Laul, 1982, The lunar regolith: chemistry, mineralogy, and petrology. Review of Geophysics and Space Physics, vol. 20, pp. 761-826.

- Pepin, R.O., L.E. Nyquist, D. Phinney, and D.C. Black, 1970, Rare gases in Apollo 11 lunar material. Proc. Apollo 11 Lunar Sci. Conf., vol. 2, pp. 1435-1454.
- Pieters, C., and T.B. McCord, 1976, Characterization of lunar mare basalt types: I. remote sensing study using reflectance spectroscopy of surface soils. Proc. 7th Lunar Sci. Conf., vol. 3, pp. 2677-2790.
- Pieters, C., J.W. Head, J.B. Adams, T.B. McCord, S. Zisk, and J. Whitford-Stark, 1980, Late high-titanium basalts of the western maria: geology of the Flamsteed region of Oceanus Procellarum. J. Geophys. Res., vol. 85, pp. 3913-3938.
- Rose, H.J., Jr., F. Cuttitta, S. Berman, F.W. Brown, M.K. Carron, R.P. Christian, E.J. Dwornik, and L.P. Greenland, 1974, Chemical composition of rocks and soils at Taurus-Littrow. Proc. 5th Lunar Sci. Conf., vol. 2, pp. 1119-1134.
- Scott, D.H., and H.A. Pohn, 1972, Geologic map of the Macrobis quadrangle of the Moon. USGS Map I-789 (LAC-43).
- Shoemaker, E.M., R.M. Batson, H.E. Holt, E.C. Morris, J.J. Renilson, and E.A. Whitaker, 1967, Television observations from Surveyor V. In Surveyor V, a preliminary report, NASA, pp. 9-42.
- Shoemaker, E.M., N.G. Bailey, N.G. Batson, R.M. Dahlem, D.H. Foss, M.J. Grolier, E.N. Goddard, M.H. Hait, H.E. Holt, K.B. Larson, K.B. Rennilson, G.E. Schaber, D.L. Schleicher, H.H. Schmitt, R.I. Sutton, G.A. Swann, A.C. Waters, and M.N. West, 1969, Geologic setting of the lunar samples obtained by the Apollo 11 mission, [chap. 3] of Apollo 11 preliminary science report: NASA Report SP-214, pp. 41-83.
- Shoemaker, E.M., M.H. Hait, G.A. Swann, D.L. Schleicher, G.C. Schaber, R.L. Sutton, D.H. Dahlem, E.N. Goddard, and A.C. Waters, 1970, Origin of the lunar regolith at Tranquility Base. Proc. Apollo 11 Lunar Sci. Conf., pp. 2399-2412.
- Shoemaker, E.M., and E.C. Morris, 1968, Size-frequency distribution of fragmental debris. Jet Propulsion Laboratory, Surveyor Project Final Report, Part II, Science Results, pp. 86-136.

- Strom, R.G., 1972, Lunar mare ridges, rings, and volcanic complexes. In the Moon Symposium 47 of the International Astronomical Union, S. Runcorn and H. Urey, eds., Reidel, Dordrecht, pp. 187-215.
- Sviatoslavsky, I.N., and M. Jacobs, 1988, Mobile helium-3 mining and extraction system. Proc. 2nd Lunar Base Conf., Houston, TX, in press.
- Vinogradov, A.P., I.K. Zadorhozny, 1972, Rare gases in the regolith from the Sea of Fertility. Space Research, vol. 13, pp. 23-311.
- Vinogradov, A.P., and I.K. Zadorhozny, 1973, Rare gases in regolith and fragments of rocks supplied by the automatic station "Luna 20". Proc. 4th Lunar Sci. Conf., vol. 2, pp. 2065-2077.
- Walton, J., S. Lakatos, and D. Heymann, 1973. Distribution of inert gases in fines from the Cayley-Descartes region. Proc. 4th Lunar Sci. Conf., vol. 2, pp. 2065-2077.
- Wakita, H., and R.A. Schmitt, 1971, Bulk elemental composition of Apollo 12 samples: five igneous rocks and one breccia, and four soils. Proc. 2nd Lunar Sci. Conf., vol. 2, pp. 1231-1236.
- Whitaker, E.A., The surface of the moon. Chap. 3 of *The Nature of the Moon* (W.N. Hess, D.H. Menzel, and J.A. O'Keefe, eds.), Proc. 1965 International Astronomical Union Symposium, Baltimore, Johns Hopkins Press, pp. 79-98.
- Wilhelms, D.E., 1972, Geologic map of the Taruntius quadrangle of the Moon. USGS Map I-722 (LAC-61).
- Wilhelms, D.E., 1987, The geological history of the Moon. U.S. Geol. Survey, Prof. Paper 1347, 302 pp.
- Willis, J.P., A.J. Erlank, J.J. Gurney, H.H. Theil, and L.H. Ahrens, 1972, Major, minor, and trace element data for some Apollo 11, 12, 14, and 15 samples. Proc. Third Lunar Sci. Conf., pp. 1269-1273.